Robust Gas Turbine and Airframe System Design in Light of Uncertain Fuel and CO_2 Prices

Stephan Langmaak[1], James Scanlan[2], and András Sóbester[3]
University of Southampton, Southampton, SO16 7QF, United Kingdom

This paper presents a study that numerically investigated which cruise speed the next generation of short-haul aircraft with 150 seats should fly at and whether a conventional two- or three-shaft turbofan, a geared turbofan, a turboprop, or an open rotor should be employed in order to make the aircraft's direct operating cost robust to uncertain fuel and carbon (CO_2) prices in the Year 2030, taking the aircraft productivity, the passenger value of time, and the modal shift into account. To answer this question, an optimization loop was set up in MATLAB consisting of nine modules covering gas turbine and airframe design and performance, flight and aircraft fleet simulation, operating cost, and optimization. If the passenger value of time is included, the most robust aircraft design is powered by geared turbofan engines and cruises at Mach 0.80. If the value of time is ignored, however, then a turboprop aircraft flying at Mach 0.70 is the optimum solution. This demonstrates that the most *fuel-efficient* option, the open rotor, is not automatically the most *cost-efficient* solution because of the relatively high engine and airframe costs.

---

[1] Research Engineer, Computational Engineering and Design
[2] Professor of Aerospace Design, Computational Engineering and Design, AIAA member
[3] Associate Professor in Aircraft Engineering, Computational Engineering and Design, AIAA member

I. Introduction

A. Background

IT takes around 5 years to develop a gas turbine engine, which then usually remains in production for more than two decades [1, 2]. Similar to the rest of the aerospace industry, gas turbine makers therefore have to make multi-billion investments into these large and long-term projects and it normally takes at least 15 years until the costs are recuperated [1]. Consequently, the strategic design team must make a sound prediction 30 years into the future and optimize the product in such a way that it remains competitive throughout that period.

The Advisory Council for Aeronautics Research in Europe (ACARE) [1] states: "The future is uncertain, except that changes will be rapid and marked, especially in the price of resources, and this scenario will become a normal phenomenon." Such uncertainties led to the development of the principle known as 'robust design', which involves a departure from the classic search for the global optimum. Instead, objective function plateaus are sought that balance nominal performance against performance variability [3]. Thus, the *System Study* presented in this paper uses a 'robust design' methodology to find the optimum cruise speed, gas turbine and airframe to minimize the direct operating cost of the next generation of short-range 150-seat aircraft in light of uncertain oil and carbon (CO_2) prices in the Year 2030.

Although 2030 is less than two decades away, this timeframe was chosen because 2025 to 2030 is the likely service entry window for the next generation of short-range aircraft [4]. In the 2020s, the engine system options described in Section II will also be mature enough to potentially be used on such an airframe. No prognosis beyond the Year 2030 is made because of the unpredictability of many factors thereafter, not just oil and carbon prices, but also technological capabilities and aircraft rollout dates [5].

1. Relevance of Work

The significance of the System Study is reflected in the richness of the literature on the subject, some of which is captured in Table 1. Although as a whole the 11 references listed in Table 1 cover most of the work carried out in the System Study, each reference primarily focuses on one of

the four sub-headings given in Table 1. Even though the System Study did not vary the aircraft capacity, the flight distance, the passenger number (i.e. the demand for air travel), nor the engine and airframe noise, the uniqueness of the methodology used lies in its all-encompassing approach to attempt to truly optimize the different engine and airframe system options to allow a fair quantitative comparison. For this reason, the model created to carry out the System Study was written entirely in MATLAB without using existing commercial or open source code.

Table 1 Literature review

Project Objectives	System Study	Cost			Environment			Uncer-tainty		Performance		
		Ref. [6]	Ref. [7]	Ref. [8]	Ref. [9]	Ref. [10]	Ref. [11]	Ref. [12]	Ref. [13]	Ref. [14]	Ref. [15]	Ref. [16]
comparison of different gas turbine systems	✓	✗	✗	✗	✗	✗	✓	✗	✓	✓	✓	✓
uncertain future fuel and CO_2 prices	✓	✗	✗	✗	✗	✗	✗	✓	✓	✗	✗	✗
optimization based on operating cost	✓	✗	✗	✗	✓	✓	✗	✓	✗	✗	✗	✗
trade-off between various engine and airframe design variables	✓	✓	✓	✗	✓	✓	✓	✓	✗	✗	✗	✗
variable aircraft capacity	✗	✗	✗	✗	✗	✓	✗	✗	✗	✗	✗	✗
various flight distances	✗	✗	✗	✗	✗	✓	✗	✓	✓	✗	✗	✗
impact of cruise speed on aircraft utilization	✓	✓	✓	✗	✗	✓	✗	✗	✗	✗	✗	✗
influence of cruise speed on the modal shift	✓	✗	✓	✗	✗	✗	✗	✗	✗	✗	✗	✗
passenger value of time	✓	✗	✓	✗	✗	✗	✗	✗	✓	✗	✗	✗
variable passenger numbers	✗	✗	✗	✗	✗	✗	✗	✓	✓	✗	✗	✗
engine and airframe noise predicted	✗	✗	✗	✗	✓	✓	✓	✗	✗	✓	✓	✗

B. Fuel Price Variability

Between 1971 and 2009, the 12-month average oil price fluctuated between \$17 and \$99 per barrel in 2012 prices, which in turn caused the fuel cost fraction to vary between 14 % and 42 % of the Direct Operating Cost (DOC) of U.S. passenger airlines [17, 18], as Fig. 1 shows. As implied by the name and defined in Table 2 in Section III, DOC is the cost directly incurred by operating

an aircraft, i.e. (1) the cost of fuel; (2) engine and airframe depreciation and maintenance costs; (3) landing, navigation, crew and ground charges. In July 2008, for example, jet fuel prices peaked at $ 4.33 per U.S. gallon, but plummeted to $ 1.28 by late December that year [19]. Similarly, between June 2014 and January 2015 the oil price dropped from around $ 110 to below $ 50 per barrel [20]. This short-term volatility is caused by market inelasticity both on the supply and the demand side, which means that small changes on either side of the economic equation have a large effect on price [21].

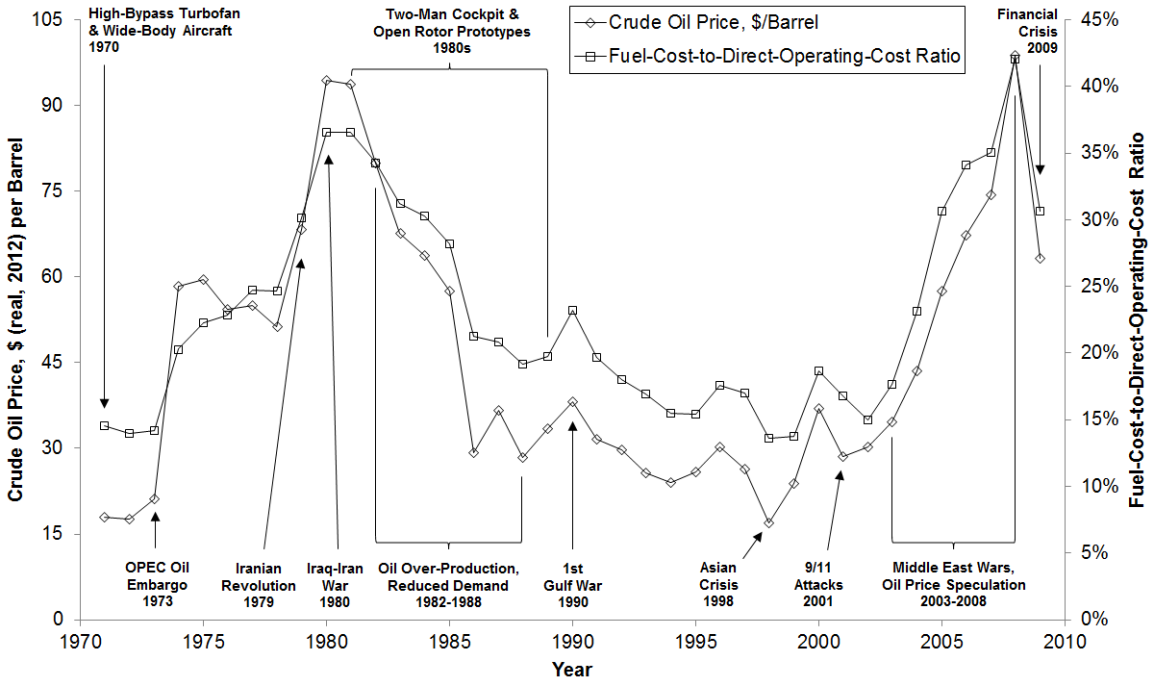

Fig. 1 Correlation between oil price and direct operating cost from 1971 to 2009 (based on data from Refs. [17, 18, 22]).

According to various forecasts, oil prices will continue to increase and exhibit increasing volatility [1, 21]. The uncertainty of future oil prices is reflected by the U.S. Energy Information Administration's (EIA) large price disparity between the best and worst case scenarios for 2030 of around 73 and 196 $/barrel in 2012 prices, respectively [18, 23]. The United Kingdom (UK) Department of Energy & Climate Change concurs with that prediction [24]. As in the past, the impact of increasing fuel prices can be minimized by efficiency gains, which, as this paper will show, is partly made possible by advanced gas turbine technology in combination with an airframe optimized for

the most cost-efficient cruise speed.

C. Carbon Trading

In 2009, the UK's House of Commons Transport Committee [4] stated that the cost of jet fuel does not provide enough incentive to achieve significant emission reductions and encourage airlines to operate the latest generation of aircraft. An additional charge is therefore required whereby 1 metric-ton of CO_2 emissions would have to cost between €100 and €300 [4], i.e. around $131 to $392 in 2012 prices [18, 25]. Based on U.S. passenger airlines data [17], in 2009 an aircraft had to fly approximately 5,400 mi on an 11-hour flight from Seattle to Beijing, for example, in order to emit 1 metric-ton of CO_2 per passenger.

As economic instruments are more cost-efficient and flexible in comparison to fixed regulation [26], the British government, the aviation industry, as well as environmental groups believe that for the international airline industry, international emission trading across all industrial sectors is the best solution [27, 28]. Since 2012, all flights within the European Union (EU) with a maximum take-off weight above 5,700 kg are therefore obliged to participate in the EU's Emission Trading Scheme [26, 29].

Considering that CO_2 was traded at approximately €6 (≈ $8) per metric-ton in 2014 [25, 30] shows that currently the EU Emission Trading Scheme has a relatively small impact on ticket prices in comparison to the fuel cost. However, the UK's Committee on Climate Change published low- and high-price scenarios for 2030 of £35 and £105 (around $62 to $186) per metric-ton of CO_2 in 2012 prices [5, 18, 25].

II. Gas Turbine and Airframe System Options

For the next-generation 150-seater, the gas turbine and airframe manufacturers are exploring five aircraft system options: the two- and three-shaft turbofan, the geared turbofan, the turboprop, and the open rotor [31–33]. Thus, this study modelled these five system options in conjunction with a fuselage, gear, flaps, slats, and spoilers based on the current Airbus A320 [34], as shown in Figs. 2–7, because it is unlikely that a radically new design, like the flying wing, will be introduced by 2030 [5, 27]. While the three turbofan options all use the conventional low-wing airframe layout where

the engines are mounted under the wing as illustrated in Figs. 2–4, the turboprop-powered aircraft displayed in Fig. 5 requires four engines installed on a high wing to provide enough ground clearance for the propeller tips. Both the wing and gear fairing in Fig. 5 are based on the BAe Avro RJ [34]. As the open rotor has two propellers mounted in tandem, Figs. 6 and 7 show that only two engines are installed at the rear of a low-wing fuselage. The difference between the aircraft in Fig. 6 and Fig. 7 is that the former is designed for a cruise speed of Mach 0.70, while the latter is optimized for Mach 0.76 which therefore has greater wing and tail sweep angles.

Each of the five system options is explained in more detail in the following sub-sections. In order to keep a clear distinction between the engine and the rest of the aircraft, the word 'airframe' is used where the term 'aircraft' might be more appropriate. Similarly, the open rotor blades are referred to as 'propellers' to avoid confusion with the rest of the engine.

A. System Option 1: Two-Shaft Turbofan

First tested on the Rolls-Royce Olympus engine in 1950 [35], the inner shaft of the two-shaft turbofan connects the slower turning fan, the low-pressure compressor (LPC), and low-pressure turbine (LPT), while the outer shaft links the high-speed high-pressure compressor (HPC) and high-pressure turbine (HPT). The two-shaft turbofan shown schematically in Fig. 2a consists of one fan, three LPC, nine HPC, two HPT, and six LPT stages. For simplicity, the shafts are not shown in Fig. 2a nor in any other engine schematic in this paper.

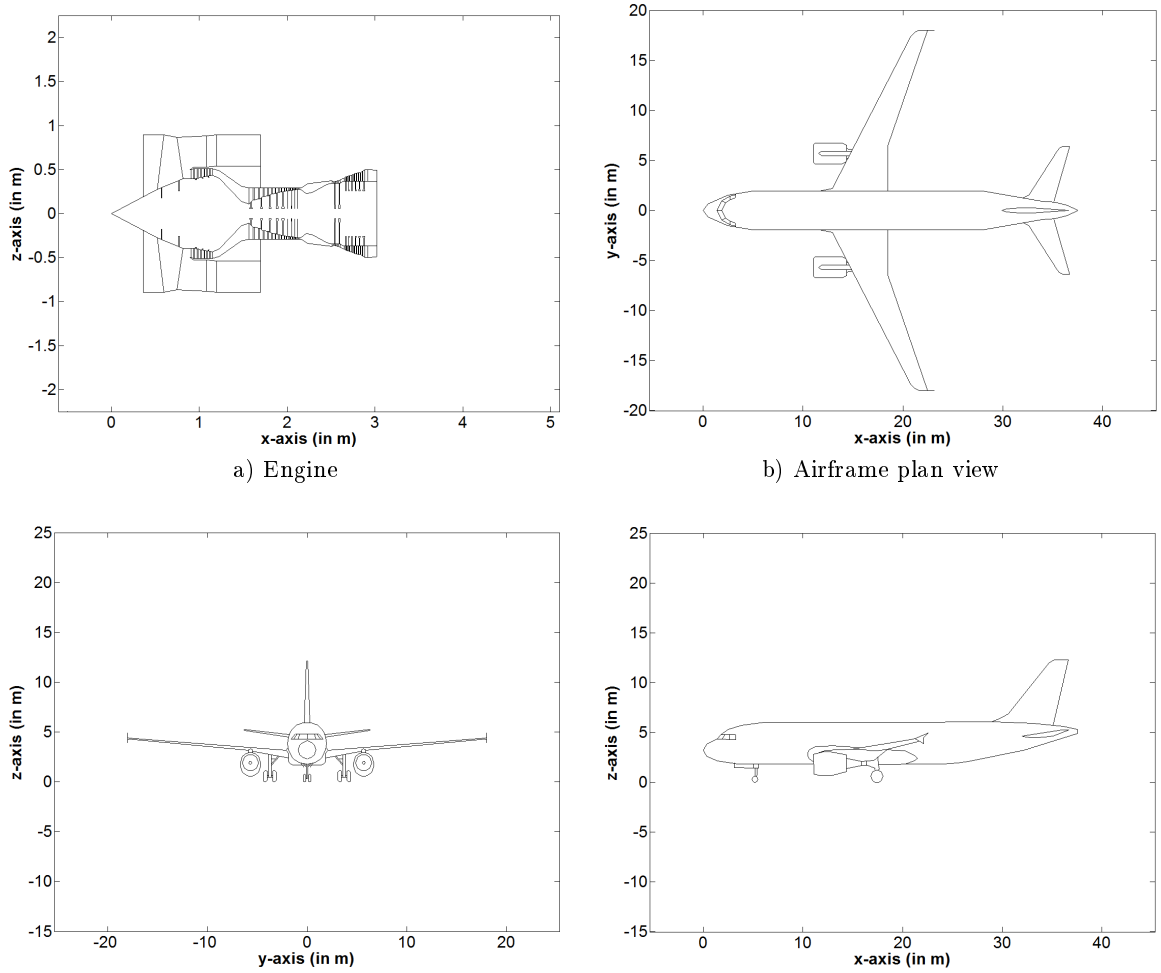

a) Engine b) Airframe plan view

c) Airframe front view d) Airframe side view

Fig. 2 Two-shaft turbofan aircraft (cruise speed: Mach 0.78).

B. System Option 2: Three-Shaft Turbofan

First certified on the RB211 engine in 1972 [36], an additional intermediate-pressure system increases efficiency and reduces engine length and weight, but leads to higher complexity and cost [2]. The three-shaft engine in Fig. 3 has one fan, seven intermediate-pressure compressor (IPC), six HPC, one HPT, one intermediate-pressure turbine (IPT), and six LPT stages.

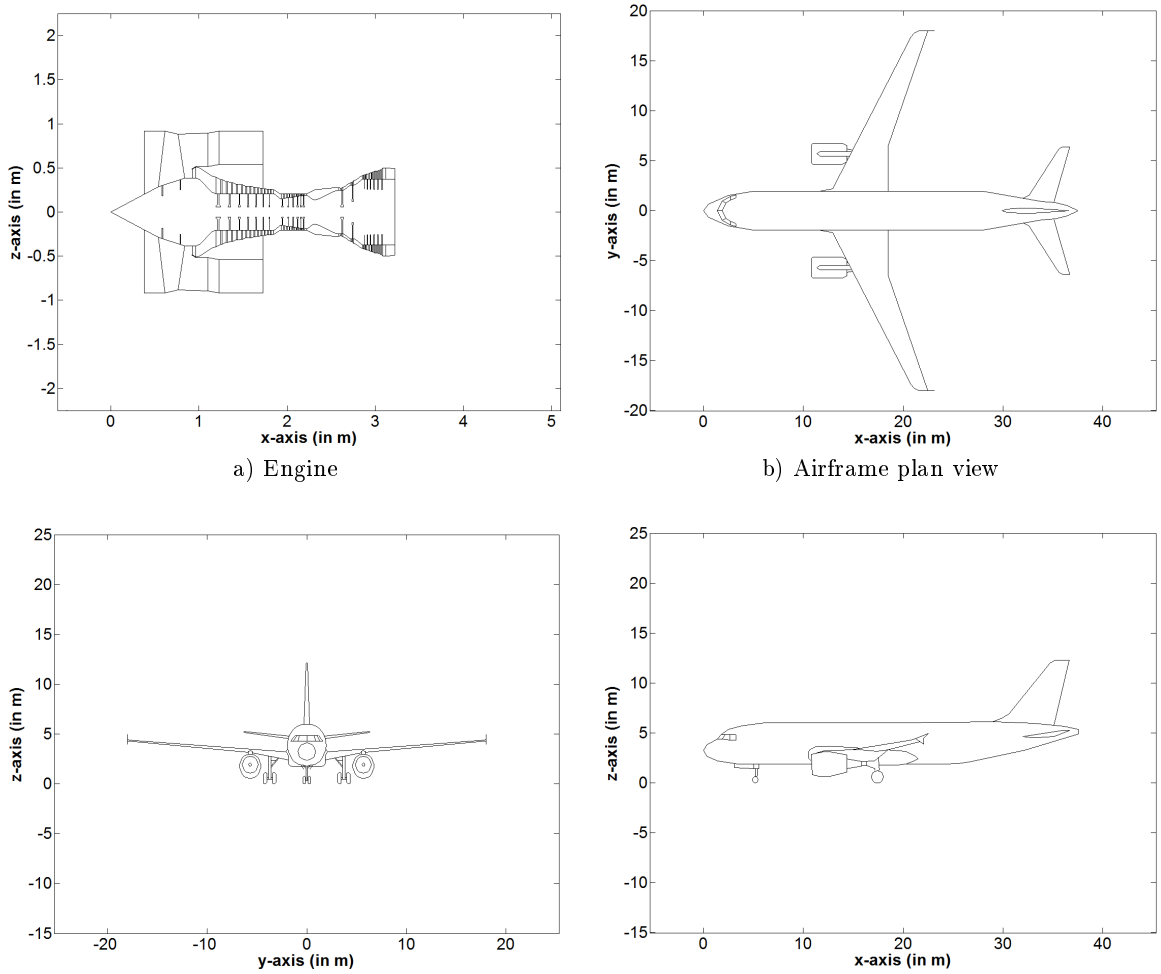

a) Engine b) Airframe plan view

c) Airframe front view d) Airframe side view

Fig. 3 Three-shaft turbofan aircraft (cruise speed: Mach 0.78).

C. System Option 3: Geared Turbofan

Instead of using a third shaft, the rotational speed of the fan can also be uncoupled from the low-pressure system by installing a planetary gear system between the fan and the LPC, as was first flight demonstrated on the Pratt & Whitney PW1000G in 2008 [37]. The effect of the planetary gear system, represented by the rectangular box between the fan and the LPC in Fig. 4a, on the engine design can clearly be seen by comparing Fig. 4a to Fig. 2a which have similar performance characteristics. Due to the increased rotational speed of the LP system, Fig. 4a only has three LPT stages while Fig. 2a has six.

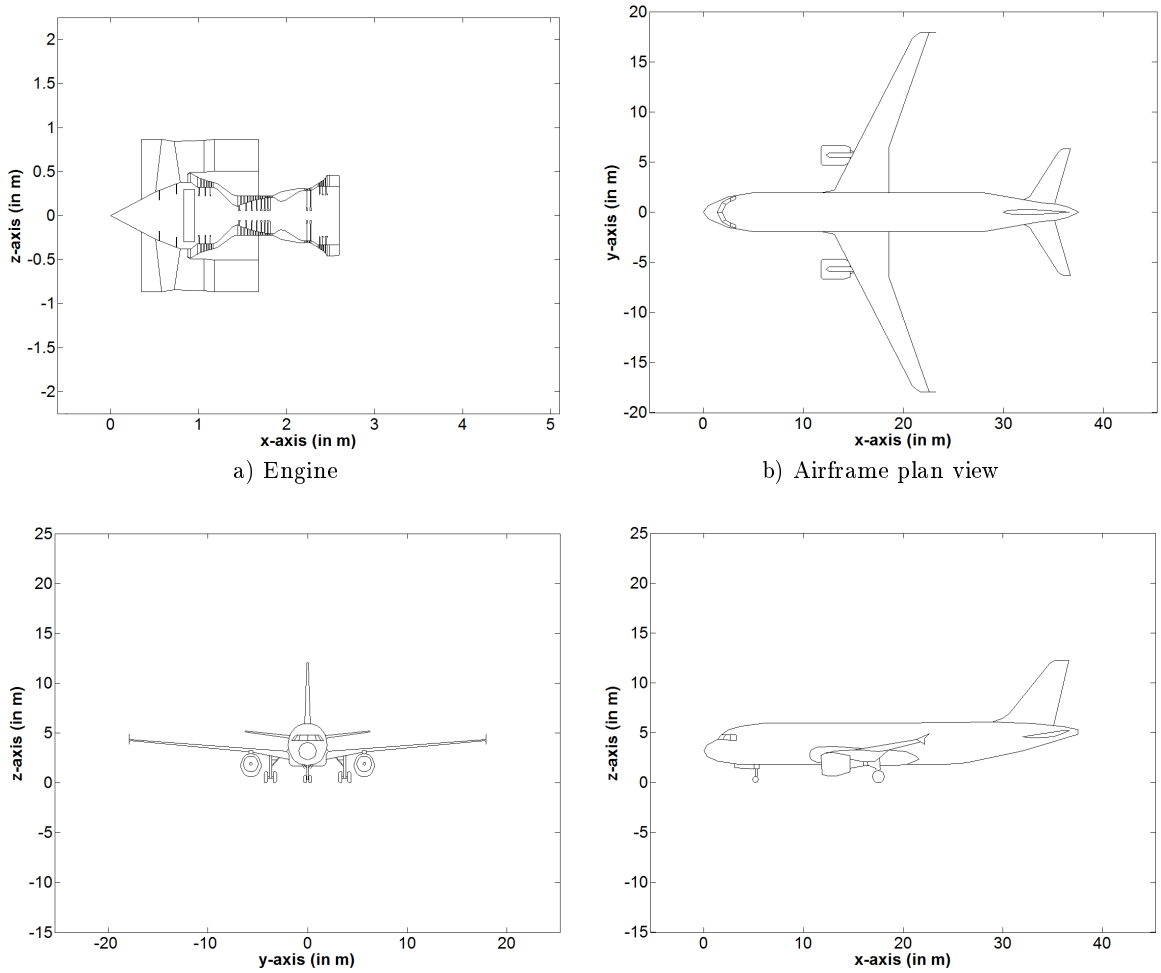

a) Engine

b) Airframe plan view

c) Airframe front view

d) Airframe side view

Fig. 4 Geared turbofan aircraft (cruise speed: Mach 0.78).

D. System Option 4: Turboprop

As the weight and the drag of the nacelle limit the bypass ratio of the turbofan, the only way to further increase efficiency is by removing the fan duct and using a propeller instead of a fan, as was first flight tested on the experimental Meteor 1 with two Rolls-Royce Trent engines in 1945 [38]. The disadvantage of removing the protective fan duct is, however, that the axial speed of the air entering the propeller is primarily determined by the flight speed, rather than by the design of the fan duct, which limits the turboprop's maximum cruise speed [2]. Similar to the geared turbofan, the propeller is driven by the LPT through a reduction gearbox in order to limit the rotational speed of the propeller and minimize the number of LPT stages. Despite the gearbox, the maximum cruise speed is also restricted to prevent the airflow velocity relative to the blade tips of the propeller

from exceeding the speed of sound, which would lead to a significant rise in noise and drag [39]. At present, the turboprop is consequently only used for shorter flights where the reduced cruise speed does not have a significant effect on the trip time [40].

The turboprop shown in Fig. 5 is based on the Europrop International TP400-D6 engine [41] which powers the Airbus A400M. Despite the higher mechanical complexity, the TP400-D6 is a three-shaft configuration because it allows the propeller to be independently powered by the LPT, while the engine core has the operational flexibility of a two-shaft engine [39, 42]. The eight-bladed propeller has a variable-pitch mechanism which means that a constant rotational speed can be maintained independently of the thrust setting by adjusting the blade pitch angle [42, 43]. The rotational speed is reduced as the cruise velocity is approached, however, to prevent the maximum flow velocity relative to the blade tips from exceeding Mach 0.95 [42]. Apart from the propeller, the engine in Fig. 5a consists of four IPC, six HPC, one HPT, one IPT, and three LPT stages.

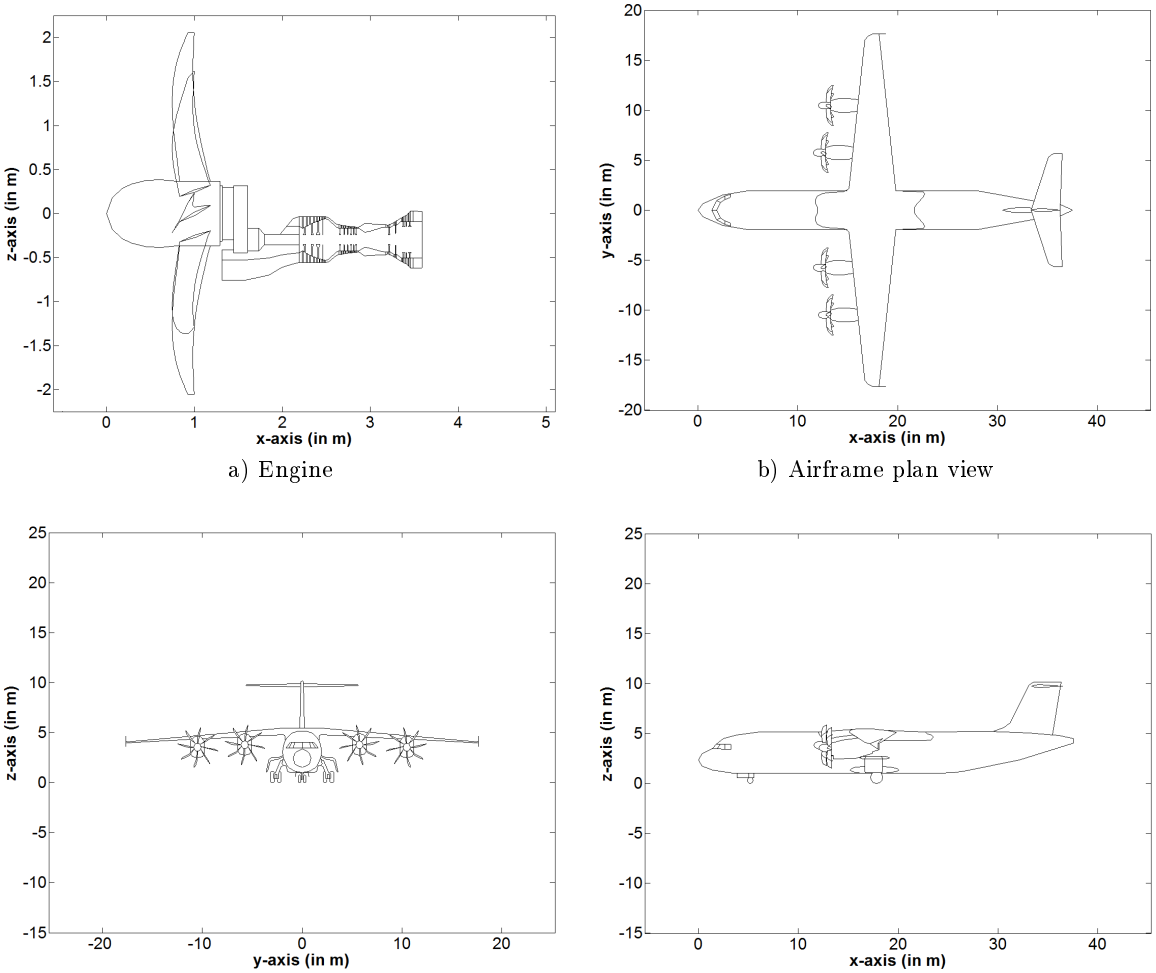

a) Engine

b) Airframe plan view

c) Airframe front view

d) Airframe side view

Fig. 5 Turboprop aircraft (cruise speed: Mach 0.70).

E. System Option 5: Open Rotor

Unlike the turboprop, the open rotor has two counter-rotating 'propellers' that are arranged in tandem. The second propeller not only increases the thrust produced, but it also recovers the air swirl leaving the first propeller, which increases engine efficiency and allows the open rotor to operate at a higher cruise speed than the turboprop [31, 39], as Fig. 7 shows. Figure 1 in Section I indicates that the open rotor concept designs were developed and tested in the 1980s as a consequence of the OPEC oil embargo of 1973 but were cancelled by the end of the decade because of the reducing oil prices [44]. Since the oil price peak in 2008, however, there has been a renewed interest in the open rotor [45].

Of the five system options, the open rotor presents the most technological and operational chal-

lenges, however, including open rotor blade integration, control and reliability, engine installation and noise [32, 46, 47]. The two propeller rows can either be installed at the front or the rear of the engine, respectively known as the tractor and the pusher configuration [31]. A further option is whether the propellers are driven directly by a counter-rotating turbine or through a reduction gearbox which requires cooling and increases mechanical complexity [47].

While the design of the ten upstream and eight downstream propeller blades in Figs. 6a and 7a is based on the EU's valiDation of Radical Engine Architecture systeMs (DREAM) project [48], the engine core is derived from Fig. 5a's turboprop but has six instead of four IPC and seven instead of six HPC stages due to the higher overall pressure ratio (see Table 5 in Section V for details). The turboprop also forms the basis of the open rotor's propeller rotational speed and blade pitch control mechanism. The geared pusher configuration was selected because of its superior performance and the lower cabin noise levels when installed at the rear of the aircraft [14, 39]. Figures 6a and 7a clearly show that the open rotor's two propellers have slightly different diameters and blade numbers to avoid blade tip vortex interference [39]. While the open rotor with the lower cruise speed is referred to as System Option (SO) 5.1, the faster one is System Option 5.2.

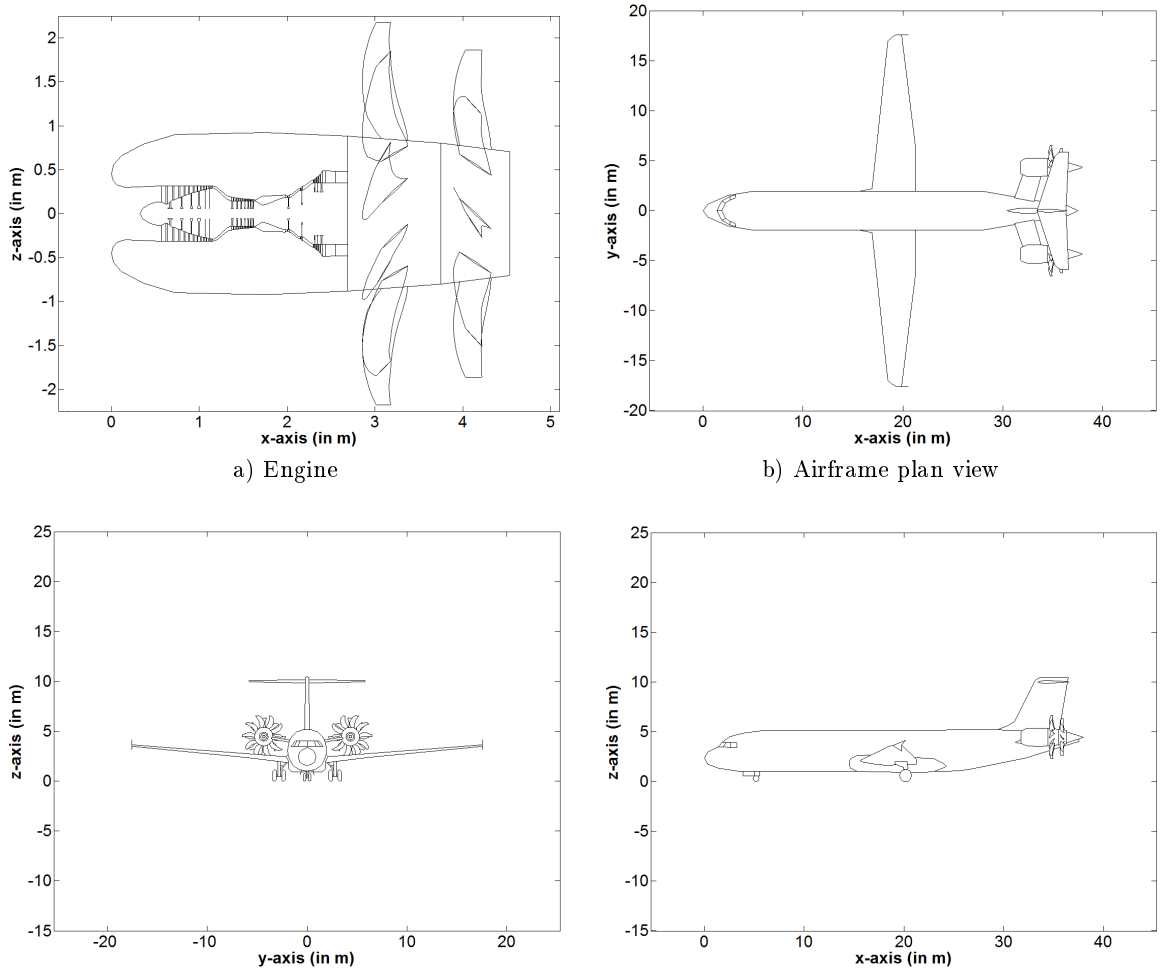

a) Engine

b) Airframe plan view

c) Airframe front view

d) Airframe side view

Fig. 6 Open rotor aircraft (cruise speed: Mach 0.70).

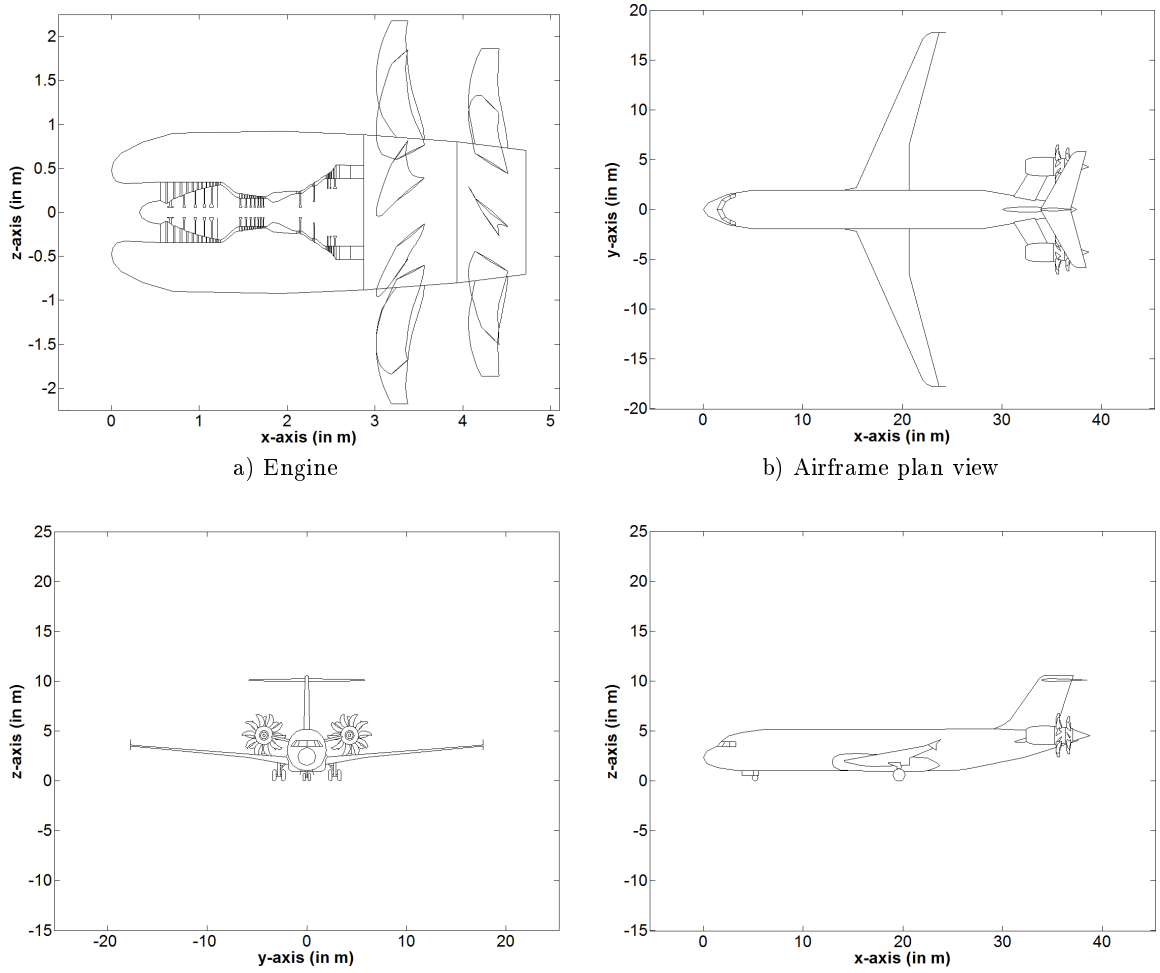

a) Engine

b) Airframe plan view

c) Airframe front view

d) Airframe side view

Fig. 7 Open rotor aircraft (cruise speed: Mach 0.76).

III. Multi-Objective Optimization

In theory, engineering design simply involves finding and analyzing all conceivable designs and then selecting the best one [49]. In order to find the best solution objectively, however, all significant design consequences have to be compared on an equal basis [50, 51]. Most real design problems have more than one objective that has to be addressed, for example minimizing cost while meeting a particular quality standard. These goals and constraints often conflict, which means that the objective functions have to be traded off in some way [51].

There are several multi-objective optimization methods available, including Objective Aggregation where all objectives are weighted and combined into one formula. Although monetary value is a form of Objective Aggregation, there are many ways of measuring and optimizing it, as the

following sub-sections show.

A. Profit

Airlines try to increase their profit by maximizing their revenue and reducing their operating costs. They consequently purchase aircraft (i.e. airframes and propulsion systems) that promise a greater profit than investing the money in other assets, i.e. competing aircraft designs or even different business ventures or financial products [52]. The profitability of the aircraft in comparison to other investments can be calculated using the Net Present Value (NPV) formula presented in Eq. 1, which is derived from Refs. [50] and [52]. It is the sum of the present values of the yearly operating profits (i.e. the yearly revenues minus the total operating costs) generated during the service life of the aircraft [52]. The depreciation of the aircraft is not included in the operating costs, because it is accounted for in the aircraft acquisition cost which is subtracted separately. While the airline revenue is primarily the sum of the passenger and freight tickets sold, the discount rate is the annual interest other investments would generate [52]. Operating cost is covered in more detail in the next sub-section.

$$NPV_P = \sum_{t=1}^{L} \left[\frac{R_t - TOC_t}{(1+i_{dis})^t} \right] - AAC \quad \text{where} \quad \begin{array}{lcl} NPV_P & = & \text{net present value of profits} \\ L & = & \text{aircraft service life in years} \\ t & = & t^{\text{th}} \text{ year of service} \\ R_t & = & \text{revenue for year } t \\ TOC_t & = & \text{total operating cost for year } t \\ & & \text{(excl. aircraft depreciation)} \\ i_{dis} & = & \text{discount rate} \\ AAC & = & \text{aircraft acquisition cost} \end{array} \tag{1}$$

The gas turbine and airframe manufacturers are more likely to maximize their sales and hence their profits if they design an aircraft that maximizes the profit of the airlines. The best aircraft design can therefore be found by maximizing Eq. 1. Net Present Value consequently enables multi-objective optimization by expressing the aircraft's specification in terms of monetary value. Rather than applying subjective weightings to incompatible design requirements, like specific fuel consumption and manufacturing cost where the optimum tradeoff is not immediately apparent, the invisible hand of the market conducts the tradeoff. This means that when specific fuel consumption is converted into fuel cost, the fuel price is used as the weighting parameter.

B. Operating Cost

The authors believe that the all-encompassing nature of Eq. 1 is its strength but also its weakness, because a large dataset is required in order to model the entire service life of the aircraft. In addition, it is particularly difficult to estimate the airline revenue because ticket prices, passenger numbers, and freight volume are controlled by many variables outside the engineering realm, including economic, geographic, political, and time factors [53]. Although fuel and carbon prices in 2030 are similarly unpredictable as airline revenues, the fuel and carbon costs of an airline are also influenced by the design of the aircraft through its fuel efficiency. Assuming that aircraft safety, noise and passenger appeal are not significantly altered, the only aircraft performance metric that has an impact on the revenue is the cruise speed. It affects the ticket prices and the number of tickets sold through the value of time and the modal shift, respectively. The value of time and the modal shift are respectively discussed in more detail in the next sub-section and in the Appendix.

Rather than modelling Eq. 1 in its entirety and obscuring the results by factors that are not related to the design of the aircraft, the focus was laid on the total operating cost. According to Doganis [54], total operating cost can be divided into direct and indirect operating costs, as shown in Table 2.

Table 2 Direct and indirect operating cost (adapted from Ref. [54])

Direct Operating Cost	Indirect Operating Cost
• aircraft depreciation (represented by AAC in Eq. 1)	• ground buildings, equipment, and transport
• interest on aircraft	• ground staff
• aircraft insurance	• ticketing, sales, and promotion
• aircraft maintenance	• administration
• fuel and oil	
• flight crew	
• cabin crew	
• airport charges	
• en-route charges	

The Indirect Operating Cost (IOC) is primarily dependent on how the airline is run and is

therefore difficult to estimate [52, 55]. For these reasons, IOC is usually ignored by the aircraft designer [55] and consequently it was also not included in this study.

The DOC, on the other hand, is significantly affected by the design of the aircraft [55]. As a figure of merit in economic analysis, aircraft comparison, and design tradeoff studies, DOC is usually expressed in $ per seat-mile or $ per revenue-passenger-kilometer (RPK) flown [52]. This accounts for the effect the load factor and the cruise speed have on the productivity of the aircraft. As DOC is effectively the value of time (aircraft and crew) and resources consumed (fuel and oil), it could also include the passengers' value of time [7]. Table 2 indicates that DOC includes aircraft depreciation, which is equivalent to dividing Eq. 1's aircraft acquisition cost by the aircraft service life, assuming that a simple linear depreciation method is used over the operating life of the aircraft. Eq. 2 shows that the NPV of the Direct Operating Costs could be calculated in a similar way as for the profits in Eq. 1. The DOC for only one year of operation was calculated, however, because the authors believe that the work involved in predicting uncertain cost data for every year of service would not improve the accuracy of the result. The futility of fully modelling both Eq. 1 and Eq. 2 is aggravated by the discount factor, which has the effect that costs incurred at the end of the service life have a diminishing effect on the NPV. A further reason why Eq. 2 was not used in this study is that the discount factor is another variable that is independent of the aircraft design.

$$NPV_{DOC} = \sum_{t=1}^{L} \left[\frac{DOC_t}{(1 + i_{dis})^t} \right] \tag{2}$$

Based on the arguments presented above, which are summarized in Table 3, the authors believe that DOC covers all the aircraft-design related aspects of Eq. 1 and is therefore a good substitute for the net present value of profits.

Table 3 Comparison of NPV_P and DOC parameters

Parameter	NPV_P	DOC
aircraft service life	t, L	aircraft depreciation
ticket price	R	value of time (the only ticket price factor directly affected by the aircraft design, assuming that aircraft safety, noise, and passenger appeal are not altered)
number of tickets sold	R	seat miles or RPK
Direct Operating Cost	TOC	included
Indirect Operating Cost	TOC	not included (not affected by the aircraft design)
discount factor	i_{dis}	not included (not affected by the aircraft design)
aircraft acquisition cost	AAC	aircraft depreciation

C. Cost of Time

Value of Time (VoT) is a concept often found in cost-benefit analyses of transport services and infrastructure [56]. In transport, it reflects how much travelers are willing to pay to save time during a journey and, conversely, how much monetary compensation they would expect for slow or delayed transport [7, 56]. As with ticket prices, the value of time depends on many factors, including the length, time, location, and itinerary of the journey, the mode of transport, the fare class, the purpose of the trip, and other socio-economic characteristics of the passenger [56, 57]. As the value of time is an opportunity cost, it only applies if the passenger has the *opportunity* to choose a faster mode of transport, i.e. in this case a competing aircraft with a higher cruise speed [7, 56, 57].

For business passengers, the value of time is equivalent to their rate of pay minus the value of the work done during the journey [56]. The value of non-working time can be found by analyzing the transport choices leisure travelers make, based on journey time and cost [56]. Business passengers generally value time higher than leisure travelers [58], which is reflected by ITA's [57] and EUROCONTROL's [59] estimates for air travel: while business passengers' average value of time is around €67 (≈ $82) per hour in 2012 prices, it is only €26 (≈ $32) per hour for tourists. Taking the passenger distribution [57, 59] into account, this gives an average value of time of €48 (≈ $58) per hour.

D. Robust Design

There are several metrics for measuring robustness in which the tradeoff between the mean and the variability of the objective function is weighted differently. While 'minimax' optimization involves minimizing the maximum value and is therefore a conservative approach because it optimizes the worst-case scenario, Bayes Principle focuses on the average-case scenario by simply minimizing the mean [3]. In this study, the Mean-Square Deviation (MSD), defined in Eq. 3, was minimized because it takes both the mean and the variability into account and is therefore a compromise between the other two approaches. Eq. 3 is adapted from Keane and Nair [3] where M represents the sample number and y_j is the j^{th} sample of the objective function.

$$MSD = \frac{1}{M}\sum_{j=1}^{M} y_j^2 \tag{3}$$

Although the reader might expect the slower but more fuel-efficient turboprop to produce the most robust design, the optimum solution is not that straightforward because of the following design tradeoffs:

- As the cruise speed affects aircraft utilization, the optimization loop has to trade productivity against fuel and carbon costs [7].
- Expensive gas turbine and airframe technology tends to reduce fuel consumption. Fuel and carbon costs therefore have to be balanced against acquisition cost [7].
- A small wing area reduces parasitic drag which tends to improve cruise performance but it leads to higher takeoff and landing speeds which requires more powerful engines [7].

The Airbus A380 has a much larger fan that increases fuel burn by 1–2 % in order to meet night-time noise restrictions at London Heathrow airport [27]. This shows that there is also a complex tradeoff between emissions and noise [31]. Noise is not included in the optimization loop, however, because of the complexity of predicting it as well as estimating its impact on the operating costs in 2030. Considering that even the open rotor is likely to meet the International Civil Aviation Organization (ICAO) Chapter 14 standard, that will take effect in 2020, shows that noise is unlikely to be a critical design factor [60].

IV. System Design Methodology and Assumptions

Figure 8 shows the optimization framework set up in MATLAB to find the most robust engine and airframe specifications for the five gas turbine options. As the exact thrust requirement for each new aircraft configuration is not known in advance, Fig. 8 indicates that Modules 1 and 2 first create provisional engine and airframe designs based on a takeoff thrust estimate of 124 kN per turbofan engine, and a turboprop and open rotor LPT power output of 5.9 MW and 18.0 MW, respectively. These thrust and power estimates are multiplied by a growth factor of 1.25 based on the thrust ratio between the growth and the baseline version of the V2500 engine [61].

These designs are then 'tested' in Module 5, which calculates how much more or less thrust is needed to meet the various performance requirements by calling Modules 3 and 4 for each scenario. The test condition with the highest relative thrust requirement defines the final engine and airframe design. This means that Modules 1 and 2 have to be rerun before Fig. 19's average flight distance (see Appendix) can be simulated in Module 6. This module calculates the total fuel consumption of the flight by running Modules 3 and 4 many times to cover the various flight stages. In Module 7, the cruise speed determines how many aircraft are needed to fly the RPKs predicted for 2030 and how much they are utilized. This information is then fed into Module 8, together with the fuel consumption and block time calculated by Module 6, to calculate the MSD of the Direct Operating Cost. Module 9's optimizer then adjusts the design variables and reruns the optimization loop until the MSD has been minimized. Although Module 9 could also optimize the cruise speed, it was varied manually outside the optimization loop to see how the robustness of the optimized designs changes with cruise velocity. Each module is described in more detail in the following sub-sections.

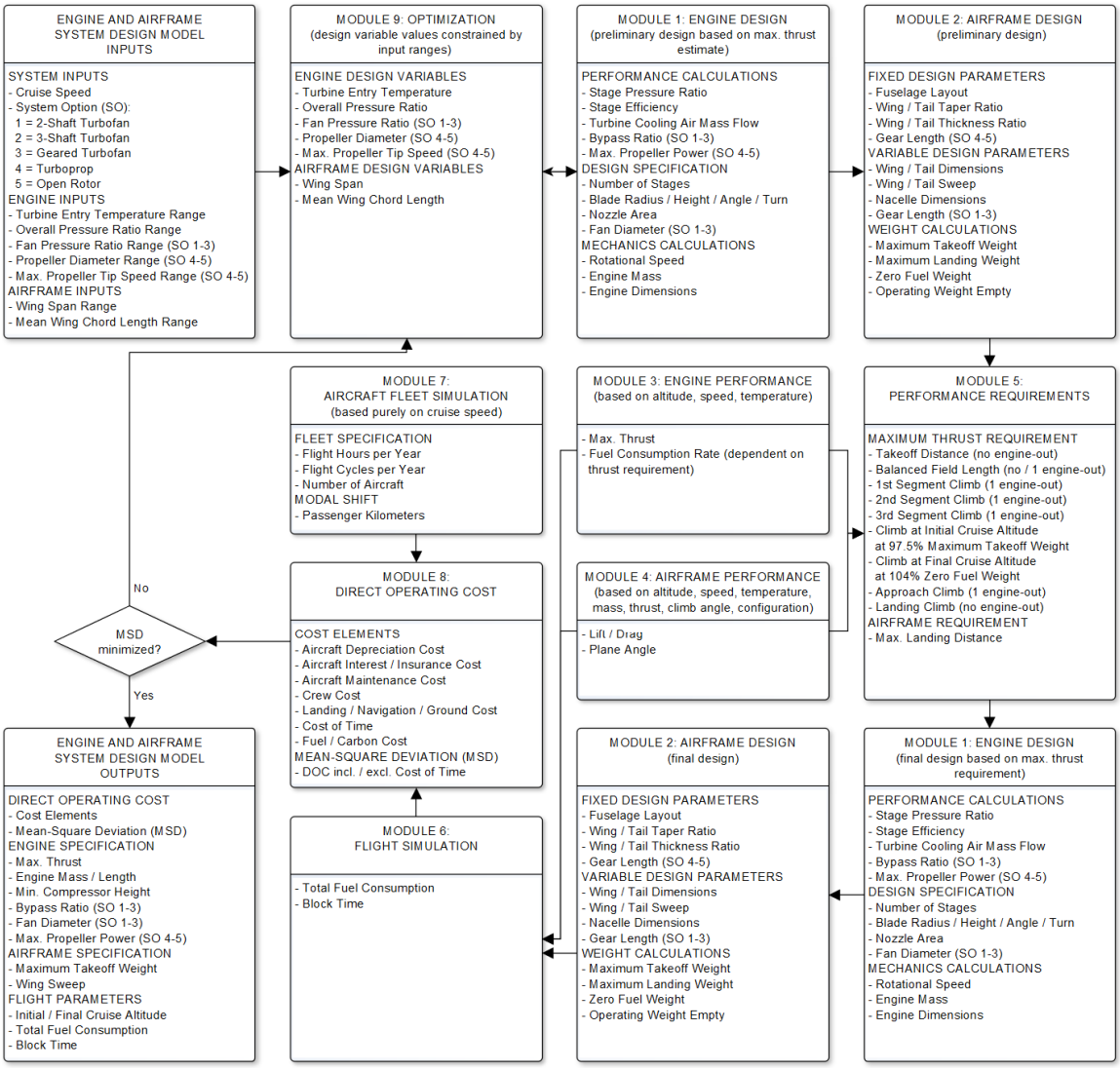

Fig. 8 System design methodology.

Table 4 lists the upper and lower limits of the design variables that the optimizer has to adhere to. While the soft constraints could be adjusted if the optimizer approached them, the hard constraints are fixed because of the physical limitations specified in Table 4. Although centrifugal compressors could alleviate the overall pressure ratio limit imposed by the minimum blade height of the axial compressor [62], these were not considered in this study.

Table 4 Design variable constraints

Design Variable	Minimum	Maximum
	Engine	
Turbine Entry Temperature	1,500 K (soft constraint)	2,000 K (hard constraint imposed by turbine material technology [31])
Overall Pressure Ratio	20 (soft constraint)	50 (soft constraint) but limited by minimum axial compressor blade height of 13 mm (hard constraint due to aerodynamic losses incurred by small compressor blades [62])
Fan Pressure Ratio	1.3 (soft constraint)	2.0 (soft constraint)
Propeller Diameter	3 m (soft constraint)	5 m (soft constraint)
Maximum Propeller Rotational Tip Speed	150 m/s (soft constraint)	350 m/s (soft constraint) but maximum relative flow velocity of Mach 0.95 (hard constraint based on TP400-D6 engine [42])
	Airframe	
Wing Span	function of minimum wing aspect ratio of 5 (hard constraint for short-range aircraft [63]) and minimum wing area (hard constraint defined by maximum approach speed of 135 kn EAS at MLW, SL, ISA[a] [64])	36 m (hard constraint to operate at ICAO Code C airports [64])
Mean Wing Chord Length	function of wing span and minimum wing area (hard constraint defined by maximum approach speed of 135 kn EAS at MLW, SL, ISA[a] [64])	function of wing span and minimum aspect ratio of 5 (hard constraint for short-range aircraft [63])

[a] kn = knots, EAS = Equivalent Airspeed, MLW = Maximum Landing Weight, SL = Sea Level ISA = International Standard Atmosphere

A. Module 1: Engine Design

The design performance of the engine, including the mass flow, velocities, pressures, temperatures, and power, are calculated by Module 1 based on the thrust requirement, the design variables specified by the optimizer and fixed component efficiencies and losses taken from Refs. [16, 62, 65, 66].

The compressor rotors and stators, including the fan for the three turbofan system options, are designed in Module 1 using velocity triangles. By calculating the mass flow, flow velocity, pressure, and temperature at each stage, the power consumed by each rotor stage can be determined, as well as the height, radius, and inlet and outlet angle of each blade. Similar computations are carried out to define the turbine, except that it also calculates how much air has to be bled off the compressor

outlet to cool the turbine blades.

While the turboprop blade design is based on the TP400-D6 propeller, the open rotor blade is derived from the DREAM project, as described in Section II. Once the blades have been scaled to the diameter specified by the optimizer, the turboprop blade is discretized into 25 elements and the two open rotor blade designs into 12 each. This ensures that the discretization error is only 0.4 % for the turboprop and 0.3 % for the open rotor. Unlike Propeller Vortex Theory, Propeller Momentum Theory and Momentum-Blade Element Theory ignore flow rotation and fail to predict no blade loading at the blade tips [43]. Propeller Vortex Theory is therefore considerably more accurate at predicting these induced effects and shows close agreement with experimental results [43].

Once the design has fully converged and satisfied various constraints, including a smooth alignment of the engine's annulus, relatively simple mechanics and the properties of five different materials, namely composite, steel, and aluminum, titanium, and nickel alloy are used to calculate the engine weight [2, 62].

B. Module 2: Airframe Design

Only the airframe's wing span and mean chord length are varied by the optimizer, because the fuselage dimensions, as well as the taper and thickness-to-chord ratios of the wing and the tail, are based on the A320, and the sweep angles of the wing and the horizontal and vertical tail are controlled by the cruise speed [34, 55]. While the diameter of the three turbofan system options is required to calculate the length of the landing gear, the turboprop's and the open rotor's propeller diameter control the minimum wing span and the pylon length, respectively. Unlike for the three turbofan system options, the gear lengths of the turboprop and open rotor aircraft are determined by the fuselage's tail-strike angle and not the propeller diameter.

The various aircraft component weights are calculated using weight formulas and fixed values given in Refs. [34, 52, 55, 63, 64, 67]. Once all the weights have been determined, they are summed up and multiplied by a weight reference factor, which calibrates the estimated Maximum Takeoff Weight (MTOW) against that of the current A320 [34]. The fact that this factor is 0.995 shows that Module 2 overpredicts the MTOW of the current A320 by only 0.5 %. Finally, the weights are

multiplied by a composite weight factor of 0.8 [55] to account for the weight reduction potential offered by composite materials.

The airframe design module re-iterates the airframe design and weight computation until the lift distribution between the wing and the horizontal tail is similar to the current Airbus A320 [34] by shifting the location of the wing and any sub-systems attached to it. This ensures that the aircraft is balanced correctly, even when the rear-fuselage mounted open rotor engines move the center of gravity of the aircraft significantly towards the rear.

C. Module 3: Engine Performance

The gas turbine performance module either calculates the engine's maximum thrust or the fuel consumption rate for a given thrust requirement. Both output options not only depend on the engine design and the performance losses specified by Module 1, but also on the atmospheric conditions. The performance computations carried out by Module 3 are identical to their counterparts in the engine design module, except that the design is fixed. Module 3 does adjust the compressor and turbine stator angles, however, to provide a smooth flow onto and off the rotor blades.

Once Module 3 has determined the engine performance for the initial turbine entry temperature, core and bypass mass flow rate, rotational speeds, and pressures, Module 3 adjusts the rotational speed of the shafts until the power consumed by the compressor sub-systems balances the power produced by respective turbine sub-systems. To ease convergence of the three-shaft systems, the IP and HP rotational speeds are linked. After the relative error has dropped below Module 3's convergence limit of 10^{-3}, Module 3 tunes the actual mass flow rate through the engine core to meet the target mass flow rate set by the core's nozzle. For the three turbofan engine options, Module 3 simultaneously modifies the bypass mass flow rate to satisfy the separate bypass nozzle conditions. If the maximum thrust has to be determined, Module 3 changes the turbine entry temperature until any of the design limits specified by Module 1 has been reached. These limits include the maximum rotational speed, the maximum turbine entry temperature, and, in the case of the turboprop engine, the LPT power limit which is set at 85 % of the maximum power output based on the TP400 derate [42]. For the alternative output option, Module 3 alters the turbine

entry temperature until the required thrust level has been met.

D. Module 4: Airframe Performance

Before Module 4 can determine the aircraft's pitch angle and lift, it has to compute the aircraft's parasitic, wave, and induced drag based on Module 2's airframe design and the drag formulas given in Ref. [52]. The aircraft's parasitic and induced drag are also affected by the configuration of the gear, flaps, slats, and spoilers, and the engine-out condition. In order to determine the pitch angle of the aircraft, Module 4 has to calculate the wing's lift slope and the lift coefficient required to balance the thrust, weight, and drag vectors. Since the pitch angle affects the thrust vector, the lift coefficient and the pitch angle are recalculated until the relative error drops below 10^{-10}.

E. Module 5: Performance Requirements

The takeoff thrust or LPT power requirement for the final engine design is calculated by multiplying the respective estimate for the provisional engine design by the maximum thrust ratio needed to meet the 10 performance requirements, adapted from Refs. [52, 64] and listed in Fig. 8. The initial and final cruise altitudes are the altitudes at which the true airspeed (in m/s) divided by the fuel consumption rate (in kg/s) is maximized, which depends on the aircraft design and weight. As a thrust ratio greater or smaller than unity affects the final engine and airframe performance, ideally, the system design should be updated until the thrust ratio converges towards 1. To save computing time, however, initial results showed that the convergence process can be approximated by raising the thrust ratio to the power of 1.3 for the three turbofan options and 1.9 for the turboprop and the open rotor.

F. Module 6: Flight Simulation

The flight profile simulated by Module 6 was adapted from Ref. [64] and is displayed in Fig. 9. It assumes ISA conditions with no temperature deviations and no winds and consists of three parts:

- the mission, which simulates the average flight distance of 1,546 km specified in the Appendix
- the continued cruise, which extends the mission's cruise by 45 minutes

- the diversion, which involves a rejected landing at the end of the mission and a 200-nautical-mile (nm) diversion to another airport

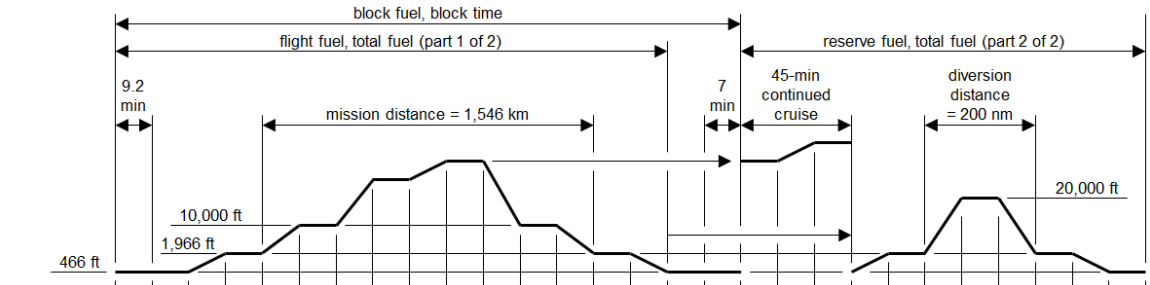

Flight Phase	taxi out	takeoff roll	takeoff ascent	acceleration	ascent	acceleration	ascent	cruise	ascent (optional)	cruise	descent	deceleration	descent	deceleration	landing approach	landing roll	taxi in	cruise	ascent (optional)	cruise	takeoff ascent	acceleration	ascent	cruise	descent	deceleration	landing approach	landing roll
Sub-Module	6.1	6.8	6.8	6.7	6.6	6.7	6.6	6.5	6.6	6.5	6.4	6.3	6.4	6.3	6.2	6.2	6.1	6.5	6.6	6.5	6.8	6.7	6.6	6.5	6.4	6.3	6.2	6.2
Flight Profile	mission																	continued cruise			diversion							
$V_{EAS,min}$ (in kn)	10	0	V_{TO}	V_{TO}	250	250	V_{max}				250	250	V_{APP}	V_{APP}	0	10	V_{max}			V_{APP}	V_{APP}	250		V_{APP}	V_{APP}	0		
$V_{EAS,max}$ (in kn)		V_{TO}		250		V_{max}						V_{max}		250	V_{APP}						250			250			V_{APP}	
Gear	down	up													down			up			up						down	
Flaps / Slats	3	0												5		0		0			5	0				5		
Spoilers	no														yes	no		no			no							yes
Thrust (in %)	7	100		75			var	75	var	7				var	var	7	var	75	var		100	75	var	7		var	var	

Fig. 9 Flight profile (partly adapted from Ref. [64]).

The mission climb and descent are carried out at the maximum equivalent airspeed, but is limited by the cruise Mach number. For a cruise Mach number of 0.78, the maximum equivalent airspeed is 300 kn, which scales proportionally with any change in the cruise Mach number. Although only the mission's block fuel consumption and block time are used for the fuel cost and value of time analysis, the reserve fuel needed for the continued cruise and diversion is also critical because it contributes to the total fuel needed at the beginning of the mission. Although most of the block fuel is included in the total fuel, the fuel consumed during the mission's landing roll and taxi-in phases is not, because it is taken from the reserve fuel.

As the total fuel quantity is not known initially, Module 6 simulates the entire flight profile backwards, starting with the diversion landing roll where the total fuel quantity is zero. To avoid confusion, the naming convention in this paper assumes a forward flight simulation and any deviation from this convention is put in single quotation marks. Figure 9 indicates that the ground altitude is 466 ft above sea level because that is the average airport altitude of the 30 biggest European cities.

The mission and diversion distances exclude the distance covered during takeoff, initial acceleration, final deceleration, and landing, because these phases are primarily needed for air maneuvers [64]. While each of the taxi, takeoff, acceleration, deceleration, and landing phases only occur once, the ascent, cruise, and descent phases are divided into multiple sectors that are simulated as follows:

- Between 1,966 and 10,000 ft, every ascent and descent phase is broken down into four sectors of equal height. Above 10,000 ft, the ascent and descent sectors are stacked at 2,000-ft intervals until the cruise altitude is reached. The performance of the aircraft is then determined at mid-height of each sector.

- For the mission and continued cruise, the cruise performance is calculated before each descent sector above 28,000 ft, so that the most fuel-efficient altitude can be selected. As before, fuel efficiency is measured by dividing the true airspeed (in m/s) by the fuel consumption rate (in kg/s).

- The mission, continued, and diversion cruise performance is updated every 100 km to accurately simulate the effect of the 'increasing' fuel quantity on the aircraft weight, drag, and fuel consumption rate.

- During the mission and continued cruise, the 'increasing' aircraft weight can make a 2,000-ft lower cruise altitude more fuel-efficient. As soon as that is the case, the aircraft ascends 2,000 ft, as illustrated in Fig. 9.

- Initially, Module 6 can only estimate the diversion cruise distance because the ascent profile is not known. Once the ascent has been simulated, however, Module 6 adjusts the cruise distance and recalculates the ascent profile until the diversion distance deviates by less than 0.1 km from the 200-nm target value. The same procedure and convergence limit is applied to meet the specified mission distance.

G. Module 7: Aircraft Fleet Simulation

In order to calculate how many single-aisle aircraft are needed to fly the 5.5 trillion RPKs predicted for 2030 [67] and determine the annual flight hours and flight cycles per aircraft, Module 7

stochastically computes how many RPKs and flight hours and cycles one aircraft accumulates over an operating year. For each flight, a random number between zero and one is sampled, which determines the number of aircraft seats, the flight distance, and the turnaround time, assuming that the three parameters are correlated and that the aircraft is stretchable between each flight. Although this is physically not possible, only simulating one aircraft instead of the entire fleet drastically reduces the computing time, while maintaining a large enough sample number to keep the error below 1 %.

The effect of the cruise speed on the modal shift, and thus the market share, is calculated using Fig. 17's Lognormal Cumulative Distribution in the Appendix based on the average door-to-door speed. This market share is then divided by the market share for the A320's current cruise speed of Mach 0.78 [34] to obtain a relative value, as displayed in Fig. 20, which is needed for Module 8's cost calculations that are described in the next sub-section.

H. Module 8: Direct Operating Cost

The objective of Module 8 is to determine the Mean Square Deviation (MSD) of the aircraft's direct operating cost to enable the optimizer to minimize the MSD. It is defined in Eq. 4 based on Eq. 3 in Section III. Although Eq. 4 includes the value of time, a second MSD is calculated that excludes the opportunity cost of time to determine the effect on the optimum design and cruise speed in a monopolistic scenario where the passenger does not have the opportunity to choose a faster mode of transport. All costs are given in U.S. cents (¢) in 2012 prices.

$$
\begin{aligned}
MSD_{DOC} \;=\; & \tfrac{1}{M}\sum_{j=1}^{M}\left[\left(ADC_{RPK}+ATC_{RPK}+ASC_{RPK}+AMC_{RPK}\right.\right.\\
& +ARC_{RPK}+ALC_{RPK}+ANC_{RPK}+AGC_{RPK}+AVC_{RPK}\\
& \left.\left.+AFC_{RPK,j}+ACC_{RPK,j}\right)/f_{market}\right]^2
\end{aligned}
$$

where

MSD_{DOC} = mean square deviation of the direct operating cost
M = number of samples (in this case 1,000)
j = j^{th} sample
ADC_{RPK} = aircraft depreciation cost per RPK (in ¢/km, 2012)
ATC_{RPK} = aircraft interest cost per RPK (in ¢/km, 2012)
ASC_{RPK} = aircraft insurance cost per RPK (in ¢/km, 2012)
AMC_{RPK} = aircraft maintenance cost per RPK (in ¢/km, 2012)
ARC_{RPK} = aircraft crew cost per RPK (in ¢/km, 2012)
ALC_{RPK} = aircraft landing cost per RPK (in ¢/km, 2012)
ANC_{RPK} = aircraft navigation cost per RPK (in ¢/km, 2012)
AGC_{RPK} = aircraft ground handling cost per RPK (in ¢/km, 2012)
AVC_{RPK} = aircraft cost of time per RPK (in ¢/km, 2012)
$AFC_{RPK,j}$ = aircraft fuel cost per RPK for sample j (in ¢/km, 2012)
$ACC_{RPK,j}$ = aircraft carbon cost per RPK for sample j (in ¢/km, 2012)
f_{market} = relative market share

(4)

The aircraft depreciation, interest, insurance, maintenance, crew, landing, navigation, and ground handling costs in Eq. 4 are calculated using equations taken from Refs. [52, 55]. While the cost of time is approximately $58/hour in 2012 prices, as quoted in Section III, the best and worst case oil price scenarios of 73 and 196 $/barrel (2012 prices), given in Section I, were modelled as a uniform uncertainty distribution using 1,000 random samples. As for the oil price, the carbon price is randomly sampled 1,000 times to create a uniform uncertainty distribution between 0 and 186 $/metric-ton of CO_2 in 2012 prices. The reason for using $0 as the lower carbon price limit, instead of the $62 specified in Section I, is to account for countries that will not have an emission trading program in 2030.

These costs are divided by Module 7's relative market share before they are squared to compute the MSD. This means that a higher market share reduces the costs and vice versa. Although a net present value calculation of the profits generated could account for the market share more realistically, Section V shows that the market share does not affect the results significantly.

I. Module 9: Optimizer

As with most design work [3], this project's objective function, the MSD of the direct operating cost, is characterized by a discontinuous relationship with the design variable inputs listed in Table 4. This is due to the fact that every gas turbine design has a discrete number of compressor and turbine stages that are subject to numerous constraints. These constraints are also the reason why the gas turbine design and performance modules become unstable if the design variables are varied randomly and consequently diverge significantly from realistic solutions, as would be the case with an evolutionary search method like the genetic algorithm [3].

For this reason, an optimization method had to be found that could search locally, starting with the V2500 engine and A320 airframe specification, but deal with multiple continuous inputs and discontinuous but deterministic outputs. The non-gradient heuristic Direct Searches satisfy these requirements because, unlike gradient-based approaches, they do not calculate the local gradient which makes them insensitive to discontinuities [3]. Although there are several other Direct Searches, the approach developed by Hooke and Jeeves [68] was chosen because of its inherent simplicity and robustness [3].

V. Results and Discussion

A. Optimum Design

Section III explains that the cruise speed affects aircraft utilization and, amongst others, the fuel and carbon costs. Due to time constraints, however, Table 5 indicates that the three turbofan options were only optimized for a cruise speed of Mach 0.78, and the turboprop and open rotor only for Mach 0.70. Visual representations of the optimum designs are shown in Figs. 2 to 6 in Section II. As none of the system options were optimized for other cruise speeds, the open rotor with the higher cruise speed of Mach 0.76, referred to as System Option 5.2 and depicted in Fig. 7, is based on System Option 5.1, i.e. the open rotor with the lower cruise speed of Mach 0.70 displayed in Fig. 6.

Table 5 Optimized system design variables and parameters

Design Variable / Parameter	SO 1: Two-Shaft Turbofan	SO 2: Three-Shaft Turbofan	SO 3: Geared Turbofan	SO 4: Turbo-prop	SO 5.1: Open Rotor
Cruise Speed (in Mach)	0.78	0.78	0.78	0.70	0.70
Turbine Entry Temperature (in K)	1,820	1,880	1,920	1,480	1,900
Overall Pressure Ratio	32.2	35.8	33.4	21.2	37.0
Fan Pressure Ratio[a]	1.80	1.78	1.78		
Propeller Diameter (in m)[b]				4.12	4.36
Max. Propeller Rotational Tip Speed (in m/s)[b]				227.2	283.2
Wing Span (in m)	36.0	36.0	35.8	35.3	35.2
Wing Mean Chord Length (in m)	3.31	3.31	3.26	3.24	3.17
Max. Static Thrust (in kN)	127.5[c]	131.4[c]	117.8[c]	58.3[d]	172.3[c]
Critical Thrust Requirement[e]	1	5	1	1	5
Max. LPT Power (in MW)[b]				5.30[d]	21.62[c]
Fan Diameter (in m)[a]	1.79	1.83	1.74		
Bypass Ratio[a,f]	6.75	7.46	7.78		
Min. Blade Height (in mm)	13.1	15.4	13.0	13.1	13.3
Engine Mass (in kg)	1,868	1,871	1,449	809	2,042
Max. Takeoff Weight (in kg)	70,232	70,280	68,870	67,541	69,241
Initial Cruise Altitude (in ft)	32,000	32,000	32,000	30,000	30,000
Final Cruise Altitude (in ft)	38,000	38,000	38,000	36,000	36,000
Mission Fuel (in kg)	4,563	4,433	4,399	3,936	3,870

[a] applies to SO 1–3

[b] applies to SO 4–5

[c] at $\Delta T = 15\,K$, includes the thrust growth factor of 1.25

[d] at $\Delta T = 15\,K$, includes the thrust growth factor of 1.25 and the max. power derate factor of 0.85

[e] 1 = takeoff field length, 2 = balanced field length, 3 = 1^{st} segment climb, 4 = 2^{nd} segment climb, 5 = 3^{rd} segment climb, 6 = initial cruise altitude, 7 = final cruise altitude (refer to Ref. [52] for details)

[f] at max. static thrust

B. Optimum Cruise Speed

Due to the similarity between the cost diagrams of the five system options, the first sub-section only shows how the costs of the two-shaft turbofan and the turboprop are affected by the cruise speed. The last two sub-sections then highlight how each system option performs relative to the others, depending on whether the value of time is included or not.

It is important to note that all charts include a relative cost of time, except where indicated, that is measured relative to the block time required when cruising at Mach 0.82, the highest cruise velocity investigated in this study. This means that a cruise speed of Mach 0.82 has a cost of time of zero, which increases as the cruise speed drops. The productivity and market share costs at the various cruise speeds are also measured relative to the cost baseline at a cruise speed of Mach 0.82. While the market share cost is the DOC multiplied by the lost market share percentage, the productivity cost is the difference between the DOC at the actual cruise speed and the DOC if the same aircraft design were flown at a cruise speed of Mach 0.82. The productivity cost is therefore dependent on the number of aircraft in the fleet as well as the annual flight hours and flight cycles per aircraft.

1. System Options

Figures 10a and 10b illustrate two conflicting cost wedges: the first one increases with cruise speed and consists of the engine, airframe, landing, navigation, crew, ground, fuel, and CO_2 costs, while the second one reduces with speed, including the productivity, market share, and time costs.

The market share cost is not significant in either of the two diagrams, because Fig. 20 in the Appendix displays that the market share only starts to decrease rapidly below a cruise speed of 400 km/h ($\approx$ Mach 0.38). Similarly, the equipment and flight costs (i.e. the engine, airframe, landing, navigation, crew, and ground costs) only increase gradually with velocity. The mean fuel and CO_2 costs, however, increase exponentially with speed due to the onset of wave drag and consequently rise more quickly at some point than the linearly reducing cost of time. The velocity at which this occurs is the optimum cruise speed if the value of time is included and varies as follows for the five system options, based on Table 6: while it is Mach 0.80 for the three turbofans, it is Mach 0.76 for the open rotor and only Mach 0.72 for the turboprop. If the value of time is ignored, however, then the minimum operating cost is at a lower speed, below which the asymptotically decreasing fuel cost saving is less than the productivity cost rise. For the three turbofan options this is Mach 0.76, while for open rotor and the turboprop it is Mach 0.70.

Table 6 Direct operating cost range (based on the cruise speeds investigated)

System Option	Optimum Cruise Speed (in Mach)		Mean DOC incl. VoT (in ¢/RPK, 2012)			Mean DOC excl. VoT (in ¢/RPK, 2012)		
	incl. VoT	excl. VoT	Rank[a]	Min.	Max.[b]	Rank[a]	Min.	Max.[b]
1	0.80	0.76	3	10.27	+2.5 %	4	9.98	+3.5 %
2	0.80	0.76	2	10.25	+2.9 %	5	10.00	+4.5 %
3	0.80	0.76	1	10.04	+2.8 %	2	9.77	+3.4 %
4	0.72	0.70	5	10.38	+3.5 %	1	9.62	+4.9 %
5	0.76	0.70	4	10.28	+5.7 %	3	9.85	+3.3 %

[a] based on minimum DOC

[b] change relative to respective minimum DOC

System Option with lowest DOC System Option with highest DOC

Table 6 displays that, in comparison to the two-shaft turbofan, System Options 2 and 3 have slightly different cost values and that the geared turbofan has the lowest DOC of all system options if the value of time is included. Despite the wide speed ranges investigated, Table 6 indicates that the biggest change in DOC (including the value of time) for the three turbofan options is only 2.9 % relative to the minimum, which increases to 4.5 % if the value of time is excluded.

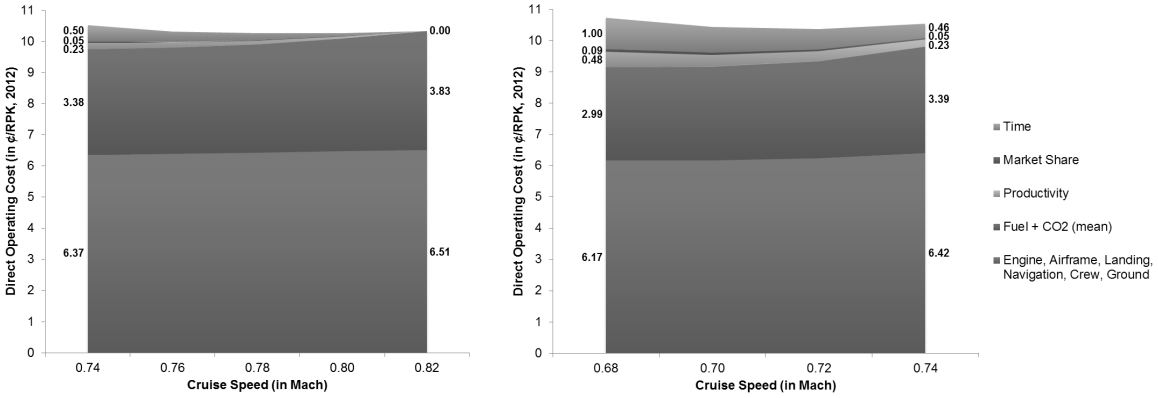

a) Two-shaft turbofan b) Turboprop

Fig. 10 Direct operating cost breakdown vs. cruise speed.

The turboprop's cost wedge in Fig. 10b has different proportions to that of the two-shaft turbofan due to the lower optimum cruise speeds and the increased fuel efficiency. Consequently, the equipment, flight, and mean fuel and CO_2 costs are lower, but the market share, productivity, and time costs are more significant. Table 6 shows that the open rotor has the largest difference between the lowest and highest DOC if the value of time is included, because System Option 5 has the widest

optimum cruise speed range. Conversely, the turboprop has the smallest range because its thrust requirement is controlled by the initial cruise altitude if the cruise speed diverges from Mach 0.70, while the open rotor's thrust remains constant as Table 5 shows that it is set by the third segment climb. Irrespective of that, the turboprop has the lowest DOC if the value of time is excluded.

2. Including the Value of Time

As implied in the name and defined in Eq. 3 in Section III, MSD is the mean of the squares of the DOC values. In order to make comparisons with the mean DOC values quoted in the previous sub-section easier, Fig. 11 presents the square root of the MSD, but including the absolute instead of the relative cost of time.

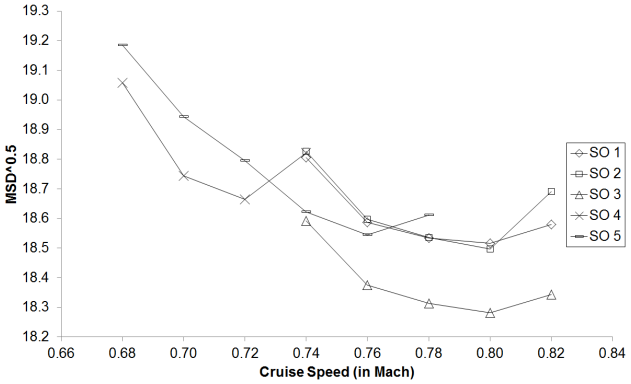

Fig. 11 System options MSD of direct operating cost (incl. value of time) vs. cruise speed.

If the value of time is included, Fig. 11 confirms that the geared turbofan has the lowest DOC of the five system options at a cruise speed of Mach 0.80 and that System Option 2 has an almost identical operating cost to System Option 1, despite a 10 % engine acquisition cost penalty imposed on the three-shaft turbofan to account for the lighter but more complex design in comparison to the two-shaft configuration. Figure 11 also highlights the turboprop's narrow optimum cruise speed range in comparison to the three turbofans and the open rotor.

Figure 12 compares the optimum system option designs, based on the minimum DOC (including the relative value of time) at Mach 0.80 for System Options 1–3, Mach 0.72 for System Option 4, and Mach 0.76 for System Option 5 to the actual DOC data of U.S. passenger airlines in the Year 2009 [17, 18]. The actual engine and airframe costs from 2009 have been blended together in Fig. 12 because

the data does not differentiate between the two. As the U.S. passenger airlines data also does not separate the productivity cost from the rest and does not include market share and time costs, none of these are shown in Fig. 12. Although the actual cost data is an average for all aircraft sizes and ages operated by U.S. passenger airlines in 2009, the comparison between the predicted and the actual DOC data nevertheless reveals that the costs estimates for 2030 are realistic, considering that Table 9 shows that the aircraft acquisition costs are forecasted to rise to balance the high fuel and CO_2 cost estimates for 2030. The actual fuel cost in 2009 is significantly less than forecasted for 2030, because in addition to supplementary CO_2 costs, the mean predicted oil price for 2030 ($\approx$ 135 \$/barrel in 2012 prices) is more than twice as high as the actual price in 2009 ($\approx$ 63 \$/barrel in 2012 prices [17, 18]). This price increase between 2009 and 2030 does not translate into a similar fuel and CO_2 cost rise in Fig. 12 due to the significantly improved fuel efficiency highlighted in Table 8. As the landing and navigation charges are dependent on the Operating Weight Empty (OWE) which, according to Table 9, is predicted to reduce, Fig. 12 indicates that these are the only costs that are expected to drop.

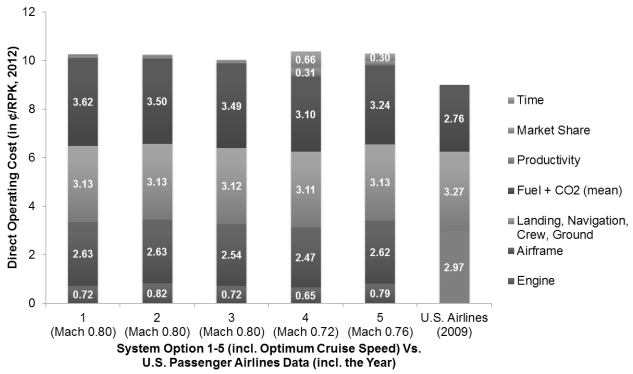

Fig. 12 Optimum system options (incl. value of time) vs. actual U.S. passenger airlines [17, 18] direct operating cost breakdown.

Focusing on the five system options, Fig. 12 confirms that the geared turbofan has the lowest operating cost if the value of time is included. Nevertheless, Table 6 shows that the turboprop, which has the highest operating cost, is only 3.4 % more expensive. Even though System Option 2 has the most costly engine, Fig. 12 illustrates that this is over-compensated by the reduced fuel consumption, making it slightly cheaper to operate than the two-shaft turbofan. However, System

Option 3 outperforms both in terms of cost efficiency because the reduced engine weight and fuel consumption also make the airframe lighter and therefore cheaper. Although the turboprop has the lowest engine cost due to the reduced turbine entry temperature and thrust requirement, the lightest and cheapest airframe and the highest fuel efficiency, the low cruise speed imposes a significant productivity and time cost, making it the most expensive option. Despite not having such a large time and productivity cost, System Option 5's high thrust and turbine entry temperature make the engine the second most expensive to operate. The high engine mass also does not help in reducing the airframe weight and hence its cost. Although the open rotor is more fuel-efficient than the geared turbofan, it has a higher fuel consumption than the turboprop due to the increased cruise speed.

3. Excluding the Value of Time

As the cost of time drops linearly with an increase in cruise speed, Fig. 13 is a tilted version of Fig. 11 in which the turboprop is the cheapest system option after being the most expensive in Fig. 11. However, as indicated in Table 6, the geared turbofan only slips down one rank to second, ahead of the open rotor and the two- and three-shaft turbofan.

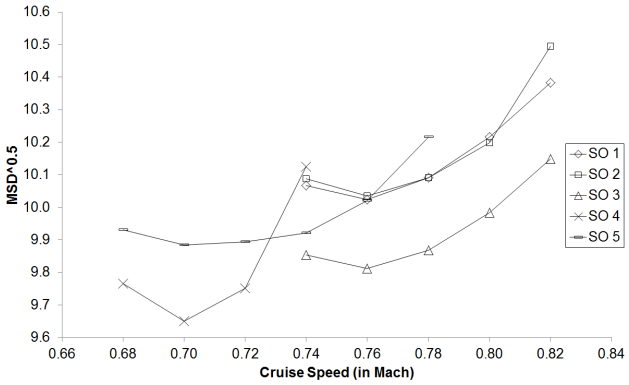

Fig. 13 System options MSD of direct operating cost (excl. value of time) vs. cruise speed.

Figure 14 looks similar to Fig. 12, except that the cost of time is not included and that most of the costs have decreased, except for a marginal rise in the productivity and market share costs due to the reduced cruise speeds. While the turboprop's cruise velocity has only dropped by Mach 0.02, the turbofans' have decreased by Mach 0.04 and the open rotor's by Mach 0.06 which explains their

more pronounced fuel cost saving. All system options have similar reductions in engine and airframe costs, however, due to the lower airframe weight and thrust requirement. As all costs, except for fuel and CO_2, have changed by similar amounts, it is not surprising that the turboprop is now the cheapest to operate without the cost of time. Similarly, the geared turbofan's lower engine and airframe weight and cost and its productivity cost advantage outweigh the open rotor's superior fuel efficiency. This shows that the most *fuel-efficient* option, the open rotor, is not automatically the most *cost-efficient* solution because of the relatively high engine and airframe costs.

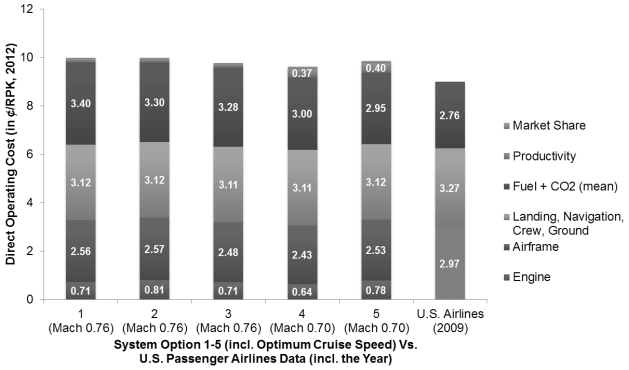

Fig. 14 Optimum system options (excl. value of time) vs. actual U.S. passenger airlines [17, 18] direct operating cost breakdown.

Table 7 shows that the $\sqrt{\text{MSD}}$ and mean DOC values are almost identical, which explains why both have the same optimum cruise speeds. The minor difference in cost is caused by the fact that, despite the uniform uncertainty distributions, $\sqrt{\text{MSD}}$ is skewed by the higher fuel and carbon cost values due to the squaring, as Eqs. 5 and 6 demonstrate for imagined values of 1.0, 1.5 and 2.0:

$$\sqrt{\text{MSD}} = \sqrt{\frac{1}{M}\sum_{j=1}^{M} y_j^2} = \sqrt{\frac{1}{3} \times (1.0^2 + 1.5^2 + 2.0^2)} = 1.55 \tag{5}$$

$$\text{Mean DOC} = \frac{1}{M}\sum_{j=1}^{M} y_j = \frac{1}{3} \times (1.0 + 1.5 + 2.0) = 1.50 \tag{6}$$

This raises the question whether it was worthwhile determining the MSD when using a uniform uncertainty distribution. The authors argue that it was, considering that the MSD provides a clear link between the fuel and carbon price ranges specified in Section I and the model, as well as a baseline against which the mean DOC could be compared.

Table 7 Comparison of optimum $\sqrt{\text{MSD}}$ and mean DOC values

System Option	$\sqrt{\text{MSD}}$ (excl. VoT)		Mean DOC (excl. VoT)	
	Cruise Speed (in Mach)	Optimum Cost (in ¢/RPK, 2012)	Cruise Speed (in Mach)	Optimum Cost (in ¢/RPK, 2012)
1	0.76	10.02	0.76	9.98
2	0.76	10.03	0.76	10.00
3	0.76	9.81	0.76	9.77
4	0.70	9.65	0.70	9.62
5	0.70	9.88	0.70	9.85

C. Verification

Table 8 proves that the optimum cruise speed and fuel consumption values presented in the previous sub-sections agree well with performance data in the public domain. It is particularly interesting to note that neither the cruise speeds of the three turbofan options nor of the turboprop deviate significantly from the Airbus A320's and A400M's current velocity, respectively, regardless of whether the value of time is included or not. The open rotor's wider speed range is also confirmed by the references given in Table 8.

Table 8 Verification of cruise speed and fuel consumption results

System Option	Cruise Speed (in Mach)		Fuel Consumption	
	System Study	Literature	System Study[a]	Literature[a]
Current Airbus A320	0.78	0.78 [34]	3.58 kg/km[b]	3.68 kg/km[c] [69]
1	0.76/0.80	0.78[d] [34]	−19.4 %/−14.2 %	−15 % [31]
2	0.76/0.80		−21.8 %/−16.9 %	
3	0.76/0.80		−22.2 %/−17.4 %	
4	0.70/0.72	0.68–0.72[e] [42]	−28.9 %/−26.4 %	
5	0.70/0.76	0.72–0.75 [14, 70]	−30.1 %/−23.1 %	−30 %/−25 % [31]

[a] percentages relative to the current Airbus A320

[b] 5,537 kg fuel for the System Study's 1,546-km mission

[c] 16,500 kg fuel for a max. range mission of 4,482 km (2,420 nm) at a MTOW of 77,000 kg

[d] based on the Airbus A320

[e] based on the Airbus A400M

According to Morrison [7], a new generation of aircraft will have an increased wing span and an increased capital cost in order to further reduce fuel consumption, as was the case in the past [8].

Both forecasts are verified by Table 9, where all system options have a greater wing span and a higher acquisition cost than the current A320. Furthermore, all system options, except for the turboprop, would have an even lower operating cost if their wing spans were allowed to exceed the limit of 36 m.

Table 9 Verification of aircraft wing span, operating weight empty, and acquisition cost results

System Option	Wing Span (in m)	Operating Weight Empty (in kg)[a]	Aircraft Acquisition Cost (in million $, 2012)[a]
Current Airbus A320	34.1 [34]	43,000 [34]	69.6 [18, 34]
1	36.0	−18.1 %	+11.2 %
2	36.0	−18.0 %	+15.2 %
3	35.8	−21.2 %	+ 8.6 %
4	35.3	−24.3 %	+ 3.7 %
5.1	35.2	−20.4 %	+11.2 %
5.2	35.3	−16.9 %	+15.1 %

[a] percentages relative to the current Airbus A320

Although Concorde was primarily retired in 2003 because of the increasing maintenance burden and the reduced passenger numbers after the Concorde crash in 2000 and the terrorist attacks of 2001, even in its hay-day the 14 Concorde aircraft only covered a niche-market [71, 72]. This was partly because the sonic boom prevented Concorde from flying supersonic over land, but primarily because it consumed six times as much fuel per passenger as a Boeing 787 today [71]. The high fuel consumption also restricted Concorde's maximum range, which meant that a scheduled non-stop service over the North Atlantic was the only viable business case [71]. Concorde's retirement followed shortly after Boeing's decision in 2002 to cancel the Sonic Cruiser in favor of the 10 % more fuel-efficient Boeing 787 despite the Sonic Cruiser's 15 % higher cruise speed of Mach 0.98 [73, 74]. This highlights that the tradeoff between the cost of fuel and the value of time has shifted towards fuel economy since the rise of oil prices in the 1970s and consequently all attempts to build a new supersonic or 'near-supersonic' passenger aircraft have failed and it is not likely to happen in the future [71].

The results presented in this study concur with the historical development of increasing fuel efficiency at the cost of a cruise speed well below Mach 1 and greater capital investment in weight-

and fuel-saving technologies like the geared turbofan and composite airframes. This development is already taking place today, as Pratt & Whitney's geared turbofan is being installed on several single-aisle aircraft and Rolls-Royce is pursuing a similar development [37, 75].

Morrison [7] also predicts that rising fuel prices will lead to a reduction in cruise speed, but this can only by verified by the results if the value of time is excluded. If the fuel and carbon prices were to increase above the range assumed in this study, however, then the higher fuel costs will have a greater leverage on the cruise speed than the value of time. Consequently, it would be more likely that the turboprop would be the cheapest aircraft to operate, regardless of whether the value of time is included or not. This would agree with Rolls-Royce's statement [33] that "there is very sound argument to be made for the majority of the 150-seat market, which flies mostly for less than 1.5 hours [being turboprop-powered]".

VI. Conclusion

As outlined in Section I, the originality of this study lies in the holistic approach of combining system design engineering and performance simulation with economic forecasting, operational research, robust design, and multi-objective optimization. This enabled five different engine and airframe system options, including the two- and three-shaft turbofan, the geared turbofan, the turboprop, and the open rotor aircraft designs to be optimized in MATLAB in terms of direct operating cost for a standard mission, so that a fair quantitative comparison could be made in light of uncertain fuel and CO_2 prices in 2030. Due to time constraints, neither a sensitivity study was carried out, nor for example whether the value of time of business travelers would justify a supersonic business jet.

The design variables optimized include the engine's turbine entry temperature, its overall pressure ratio, and the airframe's wing span and mean chord length. In addition, the three turbofan options' fan pressure ratio was varied, as well as the turboprop's and the open rotor's propeller diameter and rotational tip speed. Although the effect of the cruise speed on the system performance was also investigated, the designs were only optimized for one cruise velocity.

The cruise speed not only affects the fuel consumption, but also the productivity of the aircraft

fleet, the opportunity cost resulting from the Value of Time (VoT) of the passengers, and the market share of the aircraft in comparison to other modes of transport. All these aspects are therefore taken into account by the model, but not different aircraft sizes, flight profiles, and annual passenger numbers (i.e. demand).

The passenger VoT has a large effect on the tradeoff between the cost of fuel and the total cost of time of the aircraft, crew, and passengers: while the geared turbofan cruising at Mach 0.80 is the optimum design when the passenger VoT is taken into account, it is the turboprop at Mach 0.70 when the value of time is excluded for a monopolistic scenario in which the passenger does not have the opportunity to select a faster mode of transport. This shows that the most *fuel-efficient* option, the open rotor, is not automatically the most *cost-efficient* solution because of the relatively high engine and airframe costs.

Appendix

In order to determine how the market share of the aircraft is affected by its cruise speed, official travel time data from airline websites was collected that offered transport services between 40 European city pairs. To account for actual door-to-door times, three hours were added to the flight times, assuming that it takes one hour to get to the airport, one hour to check in and board the aircraft, and one hour to travel to the final destination [40]. Figure 15 shows these 40 door-to-door times plotted against the direct distance between the city pairs. These data points were then used to generate the linear regression line that is also displayed in Fig. 15. While the inverse of the regression line's gradient reflects today's average cruise speed of 812 km/h ($\approx$ 500 mph), the intercept of 3 hours and 40 minutes is the sum of the regressed idle time of the flights (40 minutes) and the three hours added by the authors. The regression line forms the basis of the second graph in Fig. 15, which shows how the average door-to-door speed increases with distance.

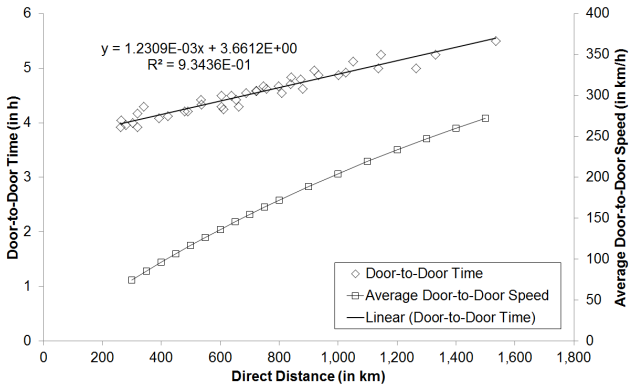

Fig. 15 Total flight journey time vs. direct distance.

Figure 16 illustrates how the market share of the aircraft, the high-speed train, and the car changes with distance, based on a diagram presented by Jenkinson et al. [55]. While the market share graphs of the aircraft and the car were constructed using the Lognormal Cumulative Distribution (LCD), the train curve simply represents the remaining market share. The distributions would probably look very different for city pairs without a high-speed train connection. By including high-speed rail rather than other slower modes of transport that compete less with air travel, however, a conservative estimate about the market share of the aircraft is being made.

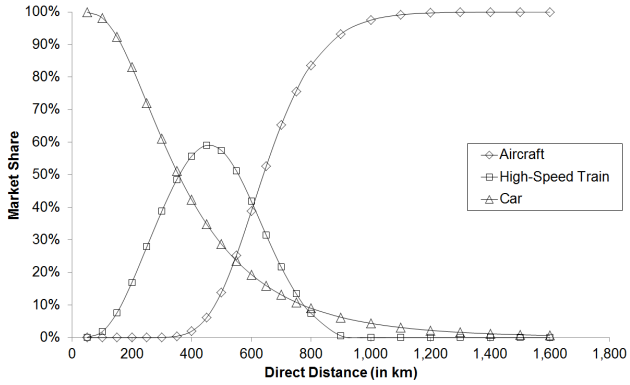

Fig. 16 Aircraft, high-speed train, and car market share vs. direct distance (data based on Ref. [55]).

The market share data shown in Fig. 16 was used in conjunction with the speed-distance relationship in Fig. 15 to derive how the aircraft's market share is related to its average door-to-door speed. Rather than using Fig. 16's LCD based on distance, the aircraft's market share can also be

described by a LCD as function of the average door-to-door speed, as Fig. 17 indicates that the two distributions overlap almost perfectly.

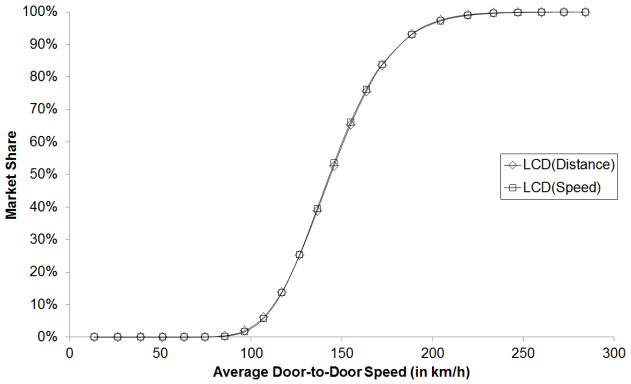

Fig. 17 Aircraft market share vs. average door-to-door speed.

Assuming that the market share of the aircraft is dependent on the average door-to-door speed, the four graphs in Fig. 18 were created by first calculating the average door-to-door times for the various cruise speeds and direct distances, and then using these in conjunction with Fig. 17's speed-based LCD to obtain the respective market shares. For cruise speeds above 600 km/h ($\approx$ 370 mph), Fig. 18 clearly shows that the aircraft becomes competitive at a direct travel distance of around 400 km ($\approx$ 250 mi) and reaches a market share above 90 % at 1,000 km ($\approx$ 620 mi) almost regardless of the cruise speed. Between 400 and 1,000 km, where the aircraft competes most with the other forms of transport, however, the cruise speed does affect the market share.

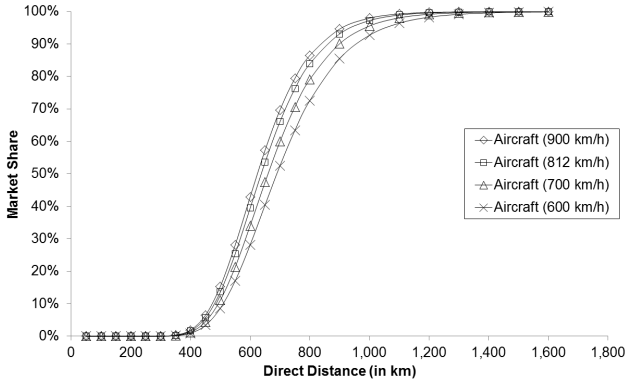

Fig. 18 Impact of cruise speed on aircraft market share.

According to Airbus [19], 70 % of single-aisle aircraft will fly 1,850 km ($\approx$ 1,150 mi) or less in

2028. This information, together with the assumption that no 150-seater flight will be less than 250 km (≈ 150 mi) but 5 % will be less than 500 km, produced the LCD shown in Fig. 19. The LCD was capped at a flight distance of 3,000 nautical miles (≈ 5,550 km / 3,450 mi) because that is the likely design range for the next-generation 150-seater [64]. Based on 10,000 stochastic samples of this distribution, the mean flight distance is 1,546 km with a standard error of 10.2 km. The standard error is a measure of the precision of the estimate and is defined as the standard deviation of the distribution divided by the square root of the sample number [76]. To save computing time, only the average flight distance was used to find the optimum engine and airframe design.

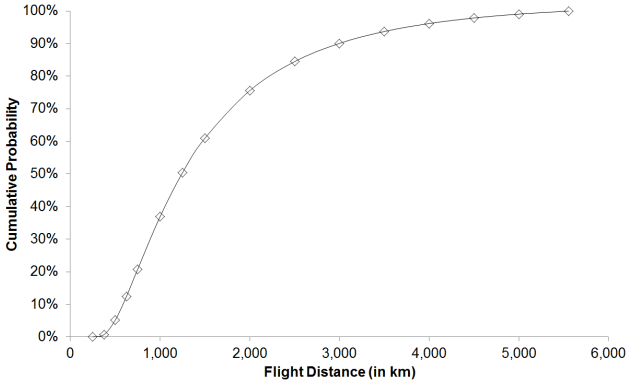

Fig. 19 Single-aisle aircraft flight distance distribution.

As Fig. 19 indicates that less than 40 % of the single-aisle flights are less than 1,000 km, Fig. 20 illustrates that the reduced market share in the 400–1,000 km segment only starts to affect the cumulative market share of the aircraft significantly if the cruise speed falls below 400 km/h. Here the cumulative market share is expressed in relative passenger-kilometers, i.e. the RPKs flown at the various speeds are divided by the RPKs flown at today's cruise speed of 812 km/h.

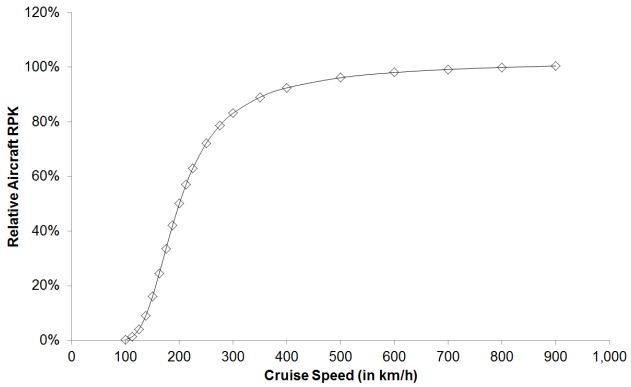

Fig. 20 Effect of cruise speed on 150-seater RPK.

Acknowledgments

This study was sponsored by Rolls-Royce plc, a power systems provider, and the United Kingdom's Engineering and Physical Sciences Research Council (EPSRC). In this context, the authors would like to thank the late Stephen Wiseall and John Whurr at Rolls-Royce, and Paul Collopy at the University of Alabama in Huntsville for their support of this project. The authors are also grateful to Phani Chinchapatnam and Sree Tammineni at Rolls-Royce, who ensured that no confidential information is published in this paper.

References

[1] Advisory Council for Aeronautics Research in Europe (ACARE), "Aeronautics and Air Transport: Beyond Vision 2020 (Towards 2050)," ACARE, 2010.

[2] Rolls-Royce, *The Jet Engine*, 6th ed., Rolls-Royce plc, London, United Kingdom, 2005.

[3] Keane, A. J., Nair, P. B., *Computational Approaches for Aerospace Design*, 1st ed., John Wiley & Sons, Chichester, United Kingdom, 2005.

[4] House of Commons Transport Committee, "The Future of Aviation," House of Commons Transport Committee, 2009.

[5] Committee on Climate Change (CCC), "Meeting the UK Aviation Target — Options for Reducing Emissions to 2050," CCC, 2009.

[6] Mentzer, W. C., Nourse, H. E., "Some Economic Aspects of Transport Airplane Performance. Part I," *Journal of the Aeronautical Sciences*, Vol. 7, No. 6, 1940, pp. 227–234.

[7] Morrison, S. A., "An Economic Analysis of Aircraft Design," *Journal of Transport Economics and Policy*, Vol. 18, No. 2, 1984, pp. 123–143.

[8] Lee, J. J., Lukachko, S. P., Waitz, I. A., Schafer, A., "Historical and Future Trends in Aircraft Performance, Cost, and Emissions," *Annual Review of Energy and the Environment*, Vol. 26, No. 1, 2001, pp. 167–200.

[9] Antoine, N., Kroo, I., Willcox, K., Barter, G., "A Framework for Aircraft Conceptual Design and Environmental Performance Studies," *10^{th} AIAA/ISSMO Multidisciplinary Analysis and Optimization Conference*, Albany, New York, USA, 2004.

[10] Bower, G. C., Kroo, I. M., "Multi-Objective Aircraft Optimization for Minimum Cost and Emissions over Specific Route Networks," *26^{th} International Congress of the Aeronautical Sciences (ICAS)*, Anchorage, Alaska, USA, 2008.

[11] Kernstine, K., Boling, B., Bortner, L., Hendricks, E., Mavris, D., "Designing for a Green Future: a Unified Aircraft Design Methodology," *Journal of Aircraft*, Vol. 47, No. 5, 2010, pp. 1789–1797.

[12] Mavris, D. N., Mantis, G. C., Kirby, M. R., "Demonstration of a Probabilistic Technique for the Determination of Aircraft Economic Viability," *SAE Transactions*, Vol. 106, No. 1, 1997, pp. 1704–1713.

[13] Ryerson, M. S., Hansen, M., "The Potential of Turboprops for Reducing Aviation Fuel Consumption," *Transportation Research Part D: Transport and Environment*, Vol. 15, No. 6, 2010, pp. 305–314.

[14] Guynn, M. D., Berton, J. J., Hendricks, E. S., Tong, M. T., Haller, W. J., "Initial Assessment of Open Rotor Propulsion Applied to an Advanced Single-Aisle Aircraft," *11^{th} AIAA Aviation Technology, Integration, and Operations Conference (ATIO)*, Virginia Beach, Virginia, USA, 2011.

[15] Peters, A., "Assessment of Propfan Propulsion Systems for Reduced Environmental Impact," M.Sc. Thesis, Massachusetts Institute of Technology, Boston, Massachusetts, USA, 2010.

[16] Hendricks, E. S., Tong, M. T., "Performance and Weight Estimates for an Advanced Open Rotor Engine," *48^{th} AIAA/ASME/SAE/ASEE Joint Propulsion Conference & Exhibit*, Atlanta, Georgia, USA, 2012.

[17] Airlines for America (A4A), "A4A Passenger Airlines Cost Index Tables," *A4A* [online], 2009, `https://publications.airlines.org/CommerceProductDetail.aspx?Product=152` [revisited 30 April 2015].

[18] Bureau of Labor Statistics, "CPI Inflation Calculator," *United States Department of Labor* [online], 2014, `http://www.bls.gov/data/inflation_calculator.htm` [revisited 30 April 2015].

[19] Airbus, "Global Market Forecast 2009–2028," Airbus S.A.S., 2009.

[20] Bowler, T., "Falling Oil Prices: Who are the Winners and Losers?," *BBC News* [online], 2015, `http://www.bbc.com/news/business-29643612` [revisited 30 April 2015].

[21] Donovan, S., Petrenas, B., Leyland, G., Caldwell, S., Barker, A., "Price Forecasts for Transport Fuels and Other Delivered Energy Forms," Auckland Regional Council, 2009.

[22] BBC News, "Oil Hits $ 100 Barrel," *BBC News* [online], 2008, `http://news.bbc.co.uk/1/hi/business/7083015.stm` [revisited 30 April 2015].

[23] U.S. Energy Information Administration (EIA), "International Energy Outlook 2013," EIA, 2013.

[24] Department of Energy & Climate Change (DECC), "DECC Fossil Fuel Price Projections," DECC, 2013.

[25] European Central Bank (ECB), "Euro Foreign Exchange Reference Rates," *ECB* [online], 2015, `http://www.ecb.europa.eu/stats/exchange/eurofxref/html/index.en.html` [revisited 30 April 2015].

[26] Scheelhaase, J. D., Grimme, W. G., "Emissions Trading for International Aviation — an Estimation of the Economic Impact on Selected European Airlines," *Journal of Air Transport Management*, Vol. 13, No. 5, 2007, pp. 253–263.

[27] Anastasi, L., Dickinson, H., Kass, G., Smith, K., Stein, C., "Aviation and the Environment," Parliamentary Office of Science and Technology (POST), 2003.

[28] Department for Transport (DfT), "The Future of Air Transport," DfT, 2003.

[29] Van Hasselt, M., Van der Zwan, F., Ghijs, S., Santema, S., "Developing a Strategic Framework for an Airline Dealing with the EU Emission Trading Scheme," *9th AIAA Aviation Technology, Integration, and Operations Conference (ATIO)*, Hilton Head, South Carolina, USA, 2009.

[30] The Guardian, "UK Calls for Cancelling of Carbon Permits to Revive EU Emissions Trading," *The Guardian* [online], 2014, `http://www.theguardian.com/environment/2014/jul/16/uk-calls-for-cancelling-of-carbon-permits-to-revive-eu-emissions-trading` [revisited 30 April 2015].

[31] Parker, R., "From Blue Skies to Green Skies: Engine Technology to Reduce the Climate-Change Impacts of Aviation," *Technology Analysis & Strategic Management*, Vol. 21, No. 1, 2009, pp. 61–78.

[32] Riegler, C., Bichlmaier, C., "The Geared Turbofan Technology — Opportunities, Challenges and Readiness Status," *1st CEAS European Air and Space Conference*, Berlin, Germany, 2007.

[33] Daly, K., "Rolls-Royce Promotes Turboprop Solution for New Civil Airliners," *Flightglobal* [online], 2008, `http://www.flightglobal.com/news/articles/rolls-royce-promotes-turboprop-solution-for-new-civil-224987/` [revisited 30 April 2015].

[34] Jackson, P. A., *Jane's All the World's Aircraft 2006–2007*, 97$^{\text{th}}$ ed., Jane's Information Group, Coulsdon, United Kingdom, 2006.

[35] Flightglobal, "Bristol Olympus," *Flightglobal* [online], 1955, `http://www.flightglobal.com/pdfarchive/view/1955/1955%20-%201753.html` [revisited 30 April 2015].

[36] Flightglobal, "R.B.211 Certificated," *Flightglobal* [online], 1972, http://www.flightglobal.com/pdfarchive/view/1972/1972%20-%200676.html [revisited 30 April 2015].

[37] Polek, G., "Pratt & Whitney Geared Turbofan Promises New Engine Dominance," *AIN-online* [online], 2013, http://www.ainonline.com/aviation-news/air-transport/2013-06-13/pratt-whitney-geared-turbofan-promises-new-engine-dominance [revisited 30 April 2015].

[38] Flightglobal, "Development of the Turboprop," *Flightglobal* [online], 1950, http://www.flightglobal.com/pdfarchive/view/1950/1950%20-%202035.html [revisited 30 April 2015].

[39] Saravanamuttoo, H. I. H., "Modern Turboprop Engines," *Progress in Aerospace Sciences*, Vol. 24, No. 3, 1987, pp. 225–248.

[40] Åkerman, J., "Sustainable Air Transport — on Track in 2050," *Transportation Research Part D: Transport and Environment*, Vol. 10, No. 2, 2005, pp. 111–126.

[41] European Aviation Safety Agency (EASA), "E.033 Europrop International GmbH TP400-D6 Engine," EASA, 2014.

[42] Jackson, P. A., *Jane's All the World's Aircraft 2011–2012*, 102nd ed., Jane's Information Group, Coulsdon, United Kingdom, 2011.

[43] McCormick, B. W., *Aerodynamics, Aeronautics, and Flight Mechanics*, 2nd ed., John Wiley & Sons, Hoboken, New Jersey, USA, 1995.

[44] Flightglobal, "Whatever Happened to Propfans," *Flightglobal* [online], 2007, http://www.flightglobal.com/news/articles/whatever-happened-to-propfans-214520/ [revisited 30 April 2015].

[45] Warwick, G., "Noise Tests Keep Promise Of Open-Rotor Engines Alive," Aviation Week, 2010.

[46] Schimming, P., "Counter Rotating Fans — an Aircraft Propulsion for the Future," *Journal of Thermal Science*, Vol. 12, No. 2, 2003, pp. 97–103.

[47] Bellocq, P., Sethi, V., Cerasi, L., Ahlefelder, S., Tantot, N., "Advanced Open Rotor Performance Modelling for Multidisciplinary Optimization Assessments," *ASME Turbo Expo 2010: Power for Land, Sea and Air*, Glasgow, United Kingdom, 2010.

[48] European Commission, "valiDation of Radical Engine Architecture systeMs (DREAM)," *European Commission* [online], 2014, http://ec.europa.eu/research/transport/news/items/dream_ip_encouraging_results_en.htm [revisited 30 April 2015].

[49] Collopy, P. D., "Economic-Based Distributed Optimal Design," *AIAA Space 2001 Conference and Exposition*, Albuquerque, New Mexico, USA, 2001.

[50] Collopy, P. D., "Surplus Value in Propulsion System Design Optimization,"

33rd AIAA/ASME/SAE/ASEE Joint Propulsion Conference & Exhibit, Seattle, Washington, USA, 1997.

[51] Hazelrigg, G. A., "A Framework for Decision-Based Engineering Design," *Journal of Mechanical Design*, Vol. 120, No. 4, 1998, pp. 653–658.

[52] Raymer, D. P., *Aircraft Design: a Conceptual Approach*, 4th ed., American Institute of Aeronautics and Astronautics Inc., Reston, Virginia, USA, 2006.

[53] Vasigh, B., Fleming, K., Tacker, T., *Introduction to Air Transport Economics: from Theory to Applications*, 1st ed., Ashgate Publishing Limited, Farnham, United Kingdom, 2008.

[54] Doganis, R., *Flying Off Course: the Economics of International Airlines*, 3rd ed., Routledge, London, United Kingdom, 2002.

[55] Jenkinson, L. R., Simpkin, P., Rhodes, D., *Civil Jet Aircraft Design*, 1st ed., Butterworth-Heinemann, Oxford, United Kingdom, 1999.

[56] Cook, A., Tanner, G., "European Airline Delay Cost Reference Values," *University of Westminster*, London, United Kingdom, 2011.

[57] Institut du Transport Aérien (ITA), "Costs of Air Transport Delay in Europe," ITA, 2000.

[58] Brons, M., Pels, E., Nijkamp, P., Rietveld, P., "Price Elasticities of Demand for Passenger Air Travel: a Meta-Analysis," *Journal of Air Transport Management*, Vol. 8, No. 3, 2002, pp. 165–175.

[59] EUROCONTROL, "Standard Inputs for EUROCONTROL Cost Benefit Analyses Edition 4.0," EUROCONTROL, 2009.

[60] Trimble, S., "Analysis: Noise Goals in Sight for Open-Rotor Researchers," *Flightglobal* [online], 2014, `http://www.flightglobal.com/news/articles/analysis-noise-goals-in-sight-for-open-rotor-researchers-395804/` [revisited 30 April 2015].

[61] European Aviation Safety Agency (EASA), "E.069 International Aero Engines AG (IAE) V2500-A5 and V2500-D5 Series Engines," EASA, 2013.

[62] Wickerson, J., "Holistic Gas Turbine," Rolls-Royce plc, 2008.

[63] Howe, D., *Aircraft Conceptual Design Synthesis*, 1st ed., Professional Engineering Publishing Limited, London and Bury St. Edmunds, United Kingdom, 2000.

[64] Airbus, "Airbus UK / University of Bath Specification for Aerospace Design Project 2007 — Low Fare Airline Optimised Aircraft," Airbus S.A.S., 2007.

[65] Mattingly, J. D., Heiser, W. H., Pratt, D. T., *Aircraft Engine Design*, 2nd ed., American Institute of Aeronautics and Astronautics Inc., Reston, Virginia, USA, 2002.

[66] Lock, G. D., "Aircraft Propulsion," University of Bath, 2006.

[67] Airbus, "Global Market Forecast 2011–2030," Airbus S.A.S., 2011.

[68] Hooke, R., Jeeves, T. A., "Direct Search Solution of Numerical and Statistical Problems," *Journal of the ACM (JACM)*, Vol. 8, No. 2, 1961, pp. 212–229.

[69] Airbus, "A320 Airplane Characteristics for Airport Planning," Airbus S.A.S., 2011.

[70] Parker, R., Lathoud, M., "Green Aero-Engines: Technology to Mitigate Aviation Impact on Environment," *Proceedings of the Institution of Mechanical Engineers, Part C: Journal of Mechanical Engineering Science*, Vol. 224, No. 3, 2010, pp. 529–538.

[71] Calder, S., "Concorde and Supersonic Travel: the Days When the Sun Rose in the West," *The Independent* [online], 2013, `http://www.independent.co.uk/travel/news-and-advice/concorde-and-supersonic-travel-the-days-when-the-sun-rose-in-the-west-8888836.html` [revisited 30 April 2015].

[72] BBC News, "Concorde Grounded for Good," *BBC News* [online], 2003, `http://news.bbc.co.uk/1/hi/uk/2934257.stm` [revisited 30 April 2015].

[73] Fagan, M., "Boeing Axes Sonic Cruiser as Airlines Lose Interest," *The Telegraph* [online], 2002, `http://www.telegraph.co.uk/finance/2837367/Boeing-axes-Sonic-Cruiser-as-airlines-lose-interest.html` [revisited 30 April 2015].

[74] Norris, G., "Sonic Cruiser is Dead — Long Live Super Efficient," *Flightglobal* [online], 2003, `http://www.flightglobal.com/news/articles/sonic-cruiser-is-dead-long-live-super-efficient-159915/` [revisited 30 April 2015].

[75] Krauskopf, L., "GE Exec Says Avoided Geared Design in Jet Engine Battle with Pratt," *Thomson Reuters* [online], 2014, `http://www.reuters.com/article/2014/09/15/us-general-electric-united-tech-engine-idUSKBN0HA2H620140915` [revisited 30 April 2015].

[76] Montgomery, D. C., Runger, G. C., *Applied Statistics and Probability for Engineers*, 3rd ed., John Wiley & Sons, Danvers, Massachusetts, USA, 2003.